Geophys. J. Int. (2003) **155,** 623–640

Modelling electromagnetic responses of 2-D structures due to spatially non-uniform inducing fields. Analysis of magnetotelluric source effects at coastlines

Patricia Martinelli* and Ana Osella*

Dto de Física, Fac. Cs. Exactas y Naturales, Universidad de Buenos Aires, Ciudad Universitaria, Pab.1, 1428, *Buenos Aires, Argentina*

Accepted 2003 June 24. Received 2003 June 24; in original form 2002 June 5

SUMMARY

In previous works, we presented 2-D and 3-D magnetotelluric modelling methods based on Rayleigh–Fourier expansions. These methods are an alternative to finite-element and finite-difference techniques and are especially suitable for modelling multilayered structures, with smooth irregular boundaries. Here we generalize the 2-D method for the calculation of the electromagnetic response of 2-D structures to arbitrary, spatially non-uniform 2-D and 3-D inducing magnetic fields. These fields are characteristic of low- and high-latitude regions. We calculate the response to different 2-D and 3-D sources, of a 2-D structure representative of the conductivity distribution which could be found at a coastline, which includes deep conductive anomalies in the lower crust and upper mantle. Then, we investigate source effects, comparing these responses to that obtained for a uniform source.

These effects become noticeable for periods greater than approximately 6 h and increase with the period of the source. They are highly dependent on the morphology of the source and also on the orientation of the external field relative to the strike direction of the structure. In various cases, they totally mask the uniform source response.

Key words: daily variations, geo-electromagnetic induction, non-uniform inducing fields, source effects.

1 INTRODUCTION

The basic hypothesis of spatially uniform (1-D) inducing magnetic fields, used for magnetotelluric (MT) modelling of the earth resistivity distribution (Tikhonov 1950; Cagniard 1953), has proved to work well in many cases, and its validity implies that the MT transfer functions depend only on the electrical structure of the earth, and not on the unknown external field. This assumption is also frequently employed to interpret data from geomagnetic deep soundings (GDS) (Schultz & Larsen 1987; Bahr & Filloux 1989). Its validity simplifies fieldwork because it implies that data do not need to be collected simultaneously at the different sounding locations. Dimitriev & Berdichevsky (1979) demonstrated that the single-site approach is also valid for sources varying linearly over length-scales exceeding the skin depth. Nevertheless, in certain cases, e.g. for studies performed at low or high latitudes, and especially for hourly or greater periods, these hypotheses usually fail due to the presence of the equatorial or auroral electrojets. When this happens, the models obtained assuming 1-D sources for the deep conductivity distribution (particularly for the lower crust and the upper and mid mantle) contain source distortions (Srivrastava 1965; Quon *et al.* 1979; Mareschal 1981; Osipova *et al.* 1989; Pirjola 1992; Vilhanen 1996; Padilha *et al.* 1997; Vilhanen *et al.* 1999).

When data are simultaneously acquired at all sounding sites it is not necessary to assume 1-D inducing fields. Some decades ago, various large 1-D or bi-dimensional (2-D) arrays of magnetometers were deployed around the world to study both the electrical structure of the crust and upper mantle and the morphology of the external magnetic field. One example is the EMSLAB array (Gough *et al.* 1989). In recent years advances in instrumentation made more feasible the simultaneous acquisition of data in 2-D arrays of fully digital MT stations, as has been done in the BEAR project in Europe (Korja 1998). Then, the development of methods to calculate the earth response to non-spatially uniform sources becomes necessary, to take full advantage of these facilities. Häkkinen & Pirjola (1986) solved the problem of tri-dimensional (3-D) inducing fields over 1-D layered earths exactly. Then, Pirjola (1992) and Vilhanen *et al.* (1993) investigated magnetotelluric source effects

*Also at: CONICET (Consejo Nacional de Investigaciones Científicas y Técnicas).

produced by inductive fields using simplified models of an auroral electrojet over a 1-D layered earth and a 2-D, two-layer (the deeper being a perfect conductor) model. Later, Boteler & Pirjola (1998) and Pirjola & Vilhanen (1998) calculated the response of 1-D layered earths to 3-D sources representing auroral electrojets using the complex image method (CIM), previously suggested by Wait & Spies (1969). Then applying the CIM, which simplifies and accelerates the calculations, Vilhanen *et al.* (1999) made a more complete study of magnetotelluric source effects over 1-D earths due to different kinds of sources associated with auroral electrojets. On the other hand, Carrasquilla & Rijo (1998) studied how source effects produced by 2-D sources representing the equatorial electrojet modify the response of 3-D conductive bodies. To do so they generalized the 3-D integral equations (IE) magnetotelluric modelling method by Wannamaker *et al.* (1984).

In a previous work, Osella & Martinelli (1993) presented a bi-dimensional MT modelling method, based on the application of Rayleigh–Fourier (RF) techniques. This method is an alternative to finite-difference (FD) (Smith & Booker 1991) and finite-element (FE) (Wannamaker *et al.* 1987) solutions. It is especially suited to modelling multilayered structures, with smooth irregular contours. Later, Osella *et al.* (1993a) generalized this method to include non-uniform, 2-D, transverse electric (TE) sources with the same strike as the 2-D structures. Using this method, Osella *et al.* (1993a,b) and Favetto *et al.* (1997) modelled the daily variations of the geomagnetic fields at Peru and Argentina, considering the morphology of the sources (in the first case, the equatorial electrojet), obtaining information concerning the regional conductivity distribution in these zones up to depths of the order of 600–800 km. Martinelli & Osella (1997) also developed a MT, 3-D, RF modelling method.

In the present paper, we extend our previous RF methods to the calculation of the electromagnetic response of this type of 2-D structure to arbitrary 2-D or 3-D inducing fields. In order to make the method even more general, and applicable to a wider range of periods than those involved in MT or induction arrays modelling (for example, such as used in controlled source soundings), we do not impose the validity of the quasi-stationary approximation in the derivations.

Then, applying this development, we perform a theoretical study of the long-period source distortions that could appear at coastlines, as a function of the morphology of the inducing fields.

2 ELECTROMAGNETIC RESPONSE OF 2-D MULTILAYERED STRUCTURES TO 3-D INDUCING FIELDS

In the following, we obtain the response of a 2-D, N-layered model, with smooth, irregular boundaries, to 3-D inducing fields. Fig. 1 shows the proposed earth model. Each medium n, for $1 \leq n \leq N$, has conductivity σ_n, dielectric permittivity ε_n and magnetic permeability μ_0 equal to that of free space. Boundaries between layers are given by functions $z = S_n(x)$. The external magnetic field, $\bar{H}^{(\mathrm{ext})}$, has a time dependence $\exp(i\omega t)$ and is a function of the coordinates x, y and z; its x and y components at the earth surface are known. Then, inside each layer n, the electric, $\bar{E}_n$ and magnetic, $\bar{H}_n$, fields satisfy (Weaver 1994)

$$\bar{\nabla} \times \bar{E}_n = -i\omega\mu_0 \bar{H}_n \tag{1}$$

$$\bar{\nabla} \times \bar{H}_n = (\sigma_n + i\omega\varepsilon_n)\bar{E}_n. \tag{2}$$

In the air (medium 0), far from the sources:

$$\bar{\nabla} \times \bar{E}_0 = -i\omega\mu_0 \bar{H}_0 \tag{3}$$

$$\bar{\nabla} \times \bar{H}_0 = i\omega\varepsilon_0 \bar{E}_0, \tag{4}$$

where ε_0 is the dielectric permittivity of vacuum.

The studied area has lengths L_x and L_y, along the x and y directions, respectively. We choose an extension of the model outside this area that simplifies the treatment. In this extended model the interfaces S_n are even and periodic functions of x, and the external magnetic

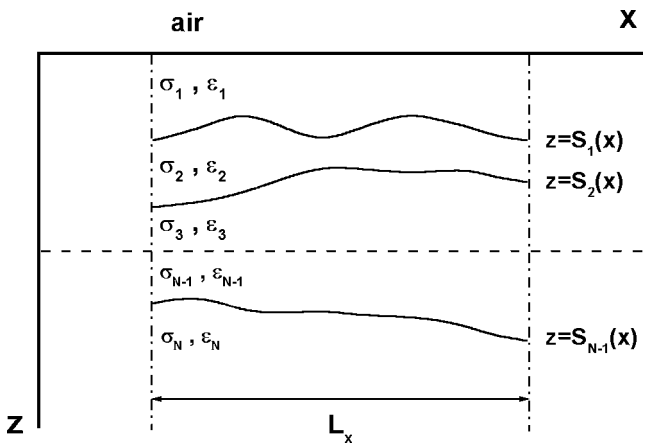

Figure 1. Generic 2-D electrical model.

field, $\bar{H}^{(\mathrm{ext})}$, is a periodic function of x and y. This external field is the sum of two contributions, $\bar{H}^{(\mathrm{ext1})}$ and $\bar{H}^{(\mathrm{ext2})}$, where the x component of $\bar{H}^{(\mathrm{ext1})}$, $H_x^{(\mathrm{ext1})}$, and the y component of $\bar{H}^{(\mathrm{ext2})}$, $H_y^{(\mathrm{ext2})}$, are even functions of x and y, and the y component of $\bar{H}^{(\mathrm{ext1})}$, $H_y^{(\mathrm{ext1})}$, and the x component of $\bar{H}^{(\mathrm{ext2})}$, $H_x^{(\mathrm{ext2})}$, are odd functions of x and y. The spatial periodicities are named λ_x and λ_y. The studied area is centred at $(x, y) = (\lambda_x/4, \lambda_y/4)$. Later, we explain in detail how we construct the extended model that satisfies these conditions. At the present, we only mention that the selected extension implies no loss of generality on the type of interfaces and external fields that can be modelled, and does not affect the results obtained in the target region, provided that λ_x and λ_y are much greater than L_x and L_y, respectively. We assume that Rayleigh scattering theory is valid on every boundary, so, the general solutions for the magnetic and electric field components, which are also periodic with x and y, can be written as the following expansions:

$$H_x^{(n)}(x, y, z, \omega) = \sum_{l,m\in Z} \left\{ A_{lm}^{(n)}(\omega) \exp\left[R_{lm}^{(n)}(\omega) z\right] + B_{lm}^{(n)}(\omega) \exp\left[-R_{lm}^{(n)}(\omega) z\right] \right\} w_l(x) v_m(y) \tag{5}$$

$$H_y^{(n)}(x, y, z, \omega) = \sum_{l,m\in Z} \left\{ C_{lm}^{(n)}(\omega) \exp\left[R_{lm}^{(n)}(\omega) z\right] + D_{lm}^{(n)}(\omega) \exp\left[-R_{lm}^{(n)}(\omega) z\right] \right\} v_l(x) w_m(y) \tag{6}$$

$$\begin{aligned} H_z^{(n)}(x, y, z, \omega) = \sum_{l,m\in Z} \frac{1}{R_{lm}^{(n)}} \Big\{ &\left[k_{xl} A_{lm}^{(n)}(\omega) + k_{ym} C_{lm}^{(n)}(\omega)\right] \exp\left[R_{lm}^{(n)}(\omega) z\right] \\ &- \left[k_{xl} B_{lm}^{(n)}(\omega) + k_{ym} D_{lm}^{(n)}(\omega)\right] \exp\left[-R_{lm}^{(n)}(\omega) z\right] \Big\} v_l(x) v_m(y) \end{aligned} \tag{7}$$

$$\begin{aligned} E_x^{(n)}(x, y, z, \omega) = \frac{i\omega\mu_0}{\gamma_n^2} \sum_{l,m\in Z} \frac{1}{R_{lm}^{(n)}} \Big\{ &\left[k_{xl} k_{ym} A_{lm}^{(n)}(\omega) - (k_{xl}^2 + \gamma_n^2) C_{lm}^{(n)}(\omega)\right] \exp\left[R_{lm}^{(n)}(\omega) z\right] \\ &- \left[k_{xl} k_{ym} B_{lm}^{(n)}(\omega) - \left(k_{xl}^2 + \gamma_n^2\right) D_{lm}^{(n)}(\omega)\right] \exp\left[-R_{lm}^{(n)}(\omega) z\right] \Big\} v_l(x) w_m(y) \end{aligned} \tag{8}$$

$$\begin{aligned} E_y^{(n)}(x, y, z, \omega) = \frac{i\omega\mu_0}{\gamma_n^2} \sum_{l,m\in Z} \frac{1}{R_{lm}^{(n)}} \Big\{ &\left[\left(k_{ym}^2 + \gamma_n^2\right) A_{lm}^{(n)}(\omega) - k_{xl} k_{ym} C_{lm}^{(n)}(\omega)\right] \exp\left[R_{lm}^{(n)}(\omega) z\right] \\ &- \left[\left(k_{ym}^2 + \gamma_n^2\right) B_{lm}^{(n)}(\omega) - k_{xl} k_{ym} D_{lm}^{(n)}(\omega)\right] \exp\left[-R_{lm}^{(n)}(\omega) z\right] \Big\} w_l(x) v_m(y) \end{aligned} \tag{9}$$

$$\begin{aligned} E_z^{(n)}(x, y, z, \omega) = \frac{i\omega\mu_0}{\gamma_n^2} \sum_{l,m\in Z} \Big\{ &\left[-k_{ym} A_{lm}^{(n)}(\omega) + k_{xl} C_{lm}^{(n)}(\omega)\right] \exp\left[R_{lm}^{(n)}(\omega) z\right] \\ &+ \left[-k_{ym} B_{lm}^{(n)}(\omega) + k_{xl} D_{lm}^{(n)}(\omega)\right] \exp\left[-R_{lm}^{(n)}(\omega) z\right] \Big\} w_l(x) w_m(y), \end{aligned} \tag{10}$$

where $\gamma_0^2 = -(\omega/c)^2$, $\gamma_n^2 = i\omega\mu_0(\sigma_n + i\omega\varepsilon_n)$, for $1 \le n \le N$, $k_{xl} = 2|l|\pi/\lambda_x$, $k_{ym} = 2|m|\pi/\lambda_y$, $[R_{lm}^{(n)}]^2 = k_{x1}^2 + k_{ym}^2 + \gamma_n^2$, and

$$v_l(x) = \begin{cases} \cos(k_{xl} x) & \text{if } l \le 0 \\ \sin(k_{xl} x) & \text{if } 0 < l \end{cases} \tag{11}$$

$$w_l(x) = \begin{cases} -\sin(k_{xl} x) & \text{if } l < 0 \\ \cos(k_{xl} x) & \text{if } 0 \le l \end{cases} \tag{12}$$

$$v_m(y) = \begin{cases} \cos(k_{ym} y) & \text{if } m \le 0 \\ \sin(k_{ym} y) & \text{if } 0 < m \end{cases} \tag{13}$$

$$w_m(y) = \begin{cases} -\sin(k_{ym} y) & \text{if } m < 0 \\ \cos(k_{ym} y) & \text{if } 0 \le m. \end{cases} \tag{14}$$

$A_{lm}^{(n)}$, $B_{lm}^{(n)}$, $C_{lm}^{(n)}$ and $D_{lm}^{(n)}$ are complex coefficients that depend on frequency ω. $B_{lm}^{(n)}$ and $D_{lm}^{(n)}$ define the incident fields and $A_{lm}^{(n)}$ and $C_{lm}^{(n)}$ the reflected ones. $B_{lm}^{(0)}$ and $D_{lm}^{(0)}$ correspond to $\bar{H}^{(\mathrm{ext})}$. $B_{lm}^{(0)}$ with $l \ge 0$ and $m \le 0$, and $D_{lm}^{(0)}$ with $l > 0$ and $m < 0$, generate $\bar{H}^{(\mathrm{ext1})}$. $B_{lm}^{(0)}$ with $l < 0$ and $m > 0$, and $D_{lm}^{(0)}$ with $l \le 0$ and $m \ge 0$, generate $\bar{H}^{(\mathrm{ext2})}$. These fields are of the form:

$$H_x^{(\mathrm{ext1})}(x, y, z, \omega) = \sum_{l\ge 0, m\le 0} B_{lm}^{(0)}(\omega) \exp\left[-R_{lm}^{(0)}(\omega) z\right] \cos(k_l x) \cos(k_m y) \tag{15}$$

$$H_y^{(\mathrm{ext1})}(x, y, z, \omega) = -\sum_{l>0, m<0} D_{lm}^{(0)}(\omega) \exp\left[-R_{lm}^{(0)}(\omega) z\right] \sin(k_l x) \sin(k_m y) \tag{16}$$

$$H_z^{(\mathrm{ext1})}(x, y, z, \omega) = -\sum_{l>0, m\le 0} \frac{1}{R_{lm}^{(0)}} \left[k_{xl} B_{lm}^{(0)}(\omega) + k_{ym} D_{lm}^{(0)}(\omega)\right] \exp\left[-R_{lm}^{(0)}(\omega) z\right] \sin(k_l x) \cos(k_m y) \tag{17}$$

$$H_x^{(\mathrm{ext2})}(x,y,z,\omega) = -\sum_{l<0,m>0} B_{lm}^{(0)}(\omega)\exp\left[-R_{lm}^{(0)}(\omega)z\right]\sin(k_l x)\sin(k_m y) \tag{18}$$

$$H_y^{(\mathrm{ext2})}(x,y,z,\omega) = \sum_{l\le 0,m\ge 0} D_{lm}^{(0)}(\omega)\exp\left[-R_{lm}^{(0)}(\omega)z\right]\cos(k_l x)\cos(k_m y) \tag{19}$$

$$H_z^{(\mathrm{ext2})}(x,y,z,\omega) = -\sum_{l\le 0,m>0} \frac{1}{R_{lm}^{(0)}}\left[k_{xl}B_{lm}^{(0)}(\omega) + k_{ym}D_{lm}^{(0)}(\omega)\right]\exp\left[-R_{lm}^{(0)}(\omega)z\right]\cos(k_l x)\sin(k_m y). \tag{20}$$

The remaining $B_{lm}^{(0)}$ and $D_{lm}^{(0)}$ are null.

It must be taken into account that Rayleigh scattering theory is an approximation valid when boundary slopes are not too large, because multiple reflections are not contemplated. In these cases, the series converge and then the coefficients corresponding to $|l|$ or $|m|$ greater than a finite value L can be neglected.

To obtain the electromagnetic response at the earth surface we apply the appropriate boundary conditions. These are the continuity of the tangential components of $\bar{E}$ and $\bar{H}$ on every interface. At $z = 0$, H_x, H_y, E_x and E_y are continuous; at $z = S_n(x)$, for $1 \le n \le N-1$:

$$\begin{aligned} &H_x^{(n)}(x,y,S_n(x),\omega) + \frac{dS_n}{dx}(x)H_z^{(n)}(x,y,S_n(x),\omega) \\ &\quad = H_x^{(n+1)}(x,y,S_n(x),\omega) + \frac{dS_n}{dx}(x)H_z^{(n+1)}(x,y,S_n(x),\omega) \end{aligned} \tag{21}$$

$$H_y^{(n)}(x,y,S_n(x),\omega) = H_y^{(n+1)}(x,y,S_n(x),\omega) \tag{22}$$

$$\begin{aligned} &E_x^{(n)}(x,y,S_n(x),\omega) + \frac{dS_n}{dx}(x)E_z^{(n)}(x,y,S_n(x),\omega) \\ &\quad = E_x^{(n+1)}(x,y,S_n(x),\omega) + \frac{dS_n}{dx}(x)E_z^{(n+1)}(x,y,S_n(x),\omega) \end{aligned} \tag{23}$$

$$E_y^{(n)}(x,y,S_n(x),\omega) = E_y^{(n+1)}(x,y,S_n(x),\omega). \tag{24}$$

In the deepest medium, N, $A_{lm}^{(N)}$ and $C_{lm}^{(N)}$ are null for every l and m because the fields must not diverge as z increases.

When these conditions are applied, we find that the responses to $\bar{H}^{(\mathrm{ext1})}$ and $\bar{H}^{(\mathrm{ext2})}$ are uncoupled. This is a direct consequence of the imposed parity of the functions $S_n(x)$. For the first external field, only the coefficients $A_{lm}^{(n)}$ and $B_{lm}^{(n)}$ corresponding to $l \ge 0$ and $m \le 0$, and the coefficients $C_{lm}^{(n)}$ and $D_{lm}^{(n)}$ corresponding to $l > 0$ and $m < 0$, differ from 0. For the second one, the non-zero coefficients are $A_{lm}^{(n)}$ and $B_{lm}^{(n)}$ corresponding to $l < 0$ and $m > 0$ and $C_{lm}^{(n)}$ and $D_{lm}^{(n)}$ corresponding to $l \le 0$ and $m \ge 0$.

Next, we calculate the response to $\bar{H}^{(\mathrm{ext1})}$.

2.1 Response to $\bar{H}^{(\mathrm{ext1})}$

$\bar{H}^{(\mathrm{ext1})}$ is defined by eqs (15)–(17). The continuity of H_x, H_y, E_x and E_y at $z = 0$ implies that, for every $l \ge 0$ and $m \le 0$:

$$A_{lm}^{(0)} + B_{lm}^{(0)}(\omega) = A_{lm}^{(1)} + B_{lm}^{(1)}(\omega) \tag{25}$$

for every $l > 0$ and $m < 0$,

$$\begin{aligned} C_{lm}^{(0)} + D_{lm}^{(0)}(\omega) &= C_{lm}^{(1)} + D_{lm}^{(1)}(\omega) \\ &\frac{1}{\gamma_0^2 R_{lm}^{(0)}}\left\{k_{xl}k_{ym}\left[A_{lm}^{(0)}(\omega) - B_{lm}^{(0)}(\omega)\right] - \left(k_{xl}^2 + \gamma_0^2\right)\left[C_{lm}^{(0)}(\omega) - D_{lm}^{(0)}(\omega)\right]\right\} \\ &= \frac{1}{\gamma_1^2 R_{lm}^{(1)}}\left\{k_{xl}k_{ym}\left[A_{lm}^{(1)}(\omega) - B_{lm}^{(1)}(\omega)\right] - \left(k_{xl}^2 + \gamma_1^2\right)\left[C_{lm}^{(1)}(\omega) - D_{lm}^{(1)}(\omega)\right]\right\} \end{aligned} \tag{26}$$

and, for every $l \ge 0$ and $m \le 0$,

$$\begin{aligned} &\frac{1}{\gamma_0^2 R_{lm}^{(0)}}\left\{\left(k_{ym}^2 + \gamma_0^2\right)\left[A_{lm}^{(0)}(\omega) - B_{lm}^{(0)}(\omega)\right] - k_{xl}k_{ym}\left[C_{lm}^{(0)}(\omega) - D_{lm}^{(0)}(\omega)\right]\right\} \\ &\quad = \frac{1}{\gamma_1^2 R_{lm}^{(1)}}\left\{\left(k_{ym}^2 + \gamma_1^2\right)\left[A_{lm}^{(1)}(\omega) - B_{lm}^{(1)}(\omega)\right] - k_{xl}k_{ym}\left[C_{lm}^{(1)}(\omega) - D_{lm}^{(1)}(\omega)\right]\right\}. \end{aligned} \tag{27}$$

At $z = S_n(x)$, for $1 \le n \le N-1$, from eq. (21), for every $m \le 0$:

$$\begin{aligned}
&\sum_{l\ge 0}\left\{A_{lm}^{(n)}(\omega)\exp\left[R_{lm}^{(n)}S_n(x)\right]+B_{lm}^{(n)}(\omega)\exp\left[-R_{lm}^{(n)}S_n(x)\right]\right\}\cos(k_{xl}x)\\
&\quad+\frac{dS_n}{dx}(x)\sum_{l>0}\frac{1}{R_{lm}^{(n)}}\left\{\left[k_{xl}A_{lm}^{(n)}(\omega)+k_{ym}C_{lm}^{(n)}(\omega)\right]\exp\left[R_{lm}^{(n)}S_n(x)\right]\right.\\
&\quad\left.-\left[k_{xl}B_{lm}^{(n)}(\omega)+k_{ym}D_{lm}^{(n)}(\omega)\right]\exp\left[-R_{lm}^{(n)}S_n(x)\right]\right\}\sin(k_{xl}x)\\
&=\sum_{l\ge 0}\left\{A_{lm}^{(n+1)}(\omega)\exp\left[R_{lm}^{(n+1)}S_n(x)\right]+B_{lm}^{(n+1)}(\omega)\exp\left[-R_{lm}^{(n+1)}S_n(x)\right]\right\}\cos(k_{xl}x)\\
&\quad+\frac{dS_n}{dx}(x)\sum_{l>0}\frac{1}{R_{lm}^{(n+1)}}\left\{\left[k_{xl}A_{lm}^{(n+1)}(\omega)+k_{ym}C_{lm}^{(n+1)}(\omega)\right]\exp\left[R_{lm}^{(n+1)}S_n(x)\right]\right.\\
&\quad\left.-\left[k_{xl}B_{lm}^{(n+1)}(\omega)+k_{ym}D_{lm}^{(n+1)}(\omega)\right]\exp\left[-R_{lm}^{(n+1)}S_n(x)\right]\right\}\sin(k_{xl}x).
\end{aligned}\tag{28}$$

From eqs (22) and (23), for every $m < 0$:

$$\begin{aligned}
&\sum_{l>0}\left\{C_{lm}^{(n)}(\omega)\exp\left[R_{lm}^{(n)}S_n(x)\right]+D_{lm}^{(n)}(\omega)\exp\left[-R_{lm}^{(n)}S_n(x)n\right]\right\}\sin(k_{xl}x)\\
&=\sum_{l>0}\left\{C_{lm}^{(n+1)}(\omega)\exp\left[R_{lm}^{(n+1)}S_n(x)\right]+D_{lm}^{(n+1)}(\omega)\exp\left[-R_{lm}^{(n+1)}S_n(x)\right]\right\}\sin(k_{xl}x)\\
&\quad\times\frac{1}{\gamma_n^2}\sum_{l>0}\frac{1}{R_{lm}^{(n)}}\left\{\left[k_{xl}k_{ym}A_{lm}^{(n)}(\omega)-(k_{xl}^2+\gamma_n^2)C_{lm}^{(n)}(\omega)\right]\exp[R_{lm}^{(n)}S_n(x)]\right.\\
&\quad\left.-\left[k_{xl}k_{ym}B_{lm}^{(n)}(\omega)-(k_{xl}^2+\gamma_n^2)D_{lm}^{(n)}(\omega)\right]\exp\left[-R_{lm}^{(n)}S_n(x)\right]\right\}\sin(k_{xl}x)\\
&\quad-\frac{1}{\gamma_n^2}\frac{dS_n}{dx}(x)\sum_{l\ge 0}\left\{\left[k_{ym}A_{lm}^{(n)}(\omega)-k_{xl}C_{lm}^{(n)}(\omega)\right]\exp\left[R_{lm}^{(n)}S_n(x)\right]\right.\\
&\quad\left.+\left[k_{ym}B_{lm}^{(n)}(\omega)-k_{xl}D_{lm}^{(n)}(\omega)\right]\exp\left[-R_{lm}^{(n)}S_n(x)\right]\right\}\cos(k_{xl}x)\\
&=\frac{1}{\gamma_{n+1}^2}\sum_{l>0}\frac{1}{R_{lm}^{(n+1)}}\left\{\left[k_{xl}k_{ym}A_{lm}^{(n+1)}(\omega)-(k_{xl}^2+\gamma_{n+1}^2)C_{lm}^{(n+1)}(\omega)\right]\exp\left[R_{lm}^{(n+1)}S_n(x)\right]\right.\\
&\quad\left.\times\left[k_{xl}k_{ym}B_{lm}^{(n+1)}(\omega)-(k_{xl}^2+\gamma_{n+1}^2)D_{lm}^{(n+1)}(\omega)\right]\exp\left[-R_{lm}^{(n+1)}S_n(x)\right]\right\}\sin(k_{xl}x)\\
&\quad-\frac{1}{\gamma_{n+1}^2}\frac{dS_n}{dx}(x)\sum_{l\ge 0}\left\{\left[k_{ym}A_{lm}^{(n+1)}(\omega)-k_{xl}C_{lm}^{(n+1)}(\omega)\right]\exp\left[R_{lm}^{(n+1)}S_n(x)\right]\right.\\
&\quad\left.+\left[k_{ym}B_{lm}^{(n+1)}(\omega)-k_{xl}D_{lm}^{(n+1)}(\omega)\right]\exp\left[-R_{lm}^{(n+1)}S_n(x)\right]n\right\}\cos(k_{xl}x),
\end{aligned}\tag{29, 30}$$

respectively. By the last, from eq. (24), for every $m \le 0$:

$$\begin{aligned}
&\frac{1}{\gamma_n^2}\sum_{l\ge 0}\frac{1}{R_{lm}^{(n)}}\left\{\left[\left(k_{ym}^2+\gamma_n^2\right)A_{lm}^{(n)}(\omega)-k_{xl}k_{ym}C_{lm}^{(n)}(\omega)\right]\exp\left[R_{lm}^{(n)}S_n(x)\right]\right.\\
&\quad\left.-\left[\left(k_{ym}^2+\gamma_n^2\right)B_{lm}^{(n)}(\omega)-k_{xl}k_{ym}D_{lm}^{(n)}(\omega)\right]\exp\left[-R_{lm}^{(n)}S_n(x)\right]\right\}\cos(k_{xl}x)\\
&=\frac{1}{\gamma_{n+1}^2}\sum_{l\ge 0}\frac{1}{R_{lm}^{(n+1)}}\left\{\left[\left(k_{ym}^2+\gamma_{n+1}^2\right)A_{lm}^{(n+1)}(\omega)-k_{xl}k_{ym}C_{lm}^{(n+1)}(\omega)\right]\exp\left[R_{lm}^{(n+1)}S_n(x)\right]\right.\\
&\quad\left.-\left[\left(k_{ym}^2+\gamma_{n+1}^2\right)B_{lm}^{(n+1)}(\omega)-k_{xl}k_{ym}D_{lm}^{(n+1)}(\omega)\right]\exp\left[-R_{lm}^{(n+1)}S_n(x)\right]\right\}\cos(k_{xl}x).
\end{aligned}\tag{31}$$

Multiplying eqs (29) and (32) by $\cos(k_{xi}x)$ for every integer number i between 0 and L, eqs (30) and (31) by $\sin(k_{xl}x)$ for every i between 1 and L, and then integrating x between $-\lambda_x/2$ and $\lambda_x/2$, we obtain systems of linear equations independent of x that can be solved independently for every m. We calculate the coefficients $A_{lm}^{(1)}$, $B_{lm}^{(1)}$, $C_{lm}^{(1)}$ and $D_{lm}^{(1)}$ that define the electromagnetic response at the Earth's surface using a procedure similar to that described in previous works (Osella & Martinelli 1993; Martinelli & Osella 1997). The RF methods proposed in these papers were extensively tested by comparison to FD, FE or IE solutions. There, a self-consistency criterion for the determination of the validity of Rayleigh's approximation in each particular case was established, which is also valid for the method presented here. When the

approximation is valid, the series expansion of field components converge, and the root mean squared values of the residual discontinuities of the tangential components at layer boundaries can be reduced to a level below a few per cent by increasing the number of scattering orders, L. In contrast, when the approximation is no longer valid, the residual discontinuities remain large, and the series directly exhibit an oscillatory behaviour, or they converge for small values of L and then become divergent as L increases. The maximum boundary slopes that can be correctly modelled using RF techniques lie typically in the range 50°–60°, but can exceed these values in very resistive cases.

2.2 Response to $\bar{H}^{(\mathrm{ext2})}$

In this case, the external field is defined by eqs (18)–(20). The continuity of the tangential components of $\bar{H}$ and $\bar{E}$, at $z = 0$, implies that eqs (25) and (28) are valid, for every $l < 0$ and $m > 0$, and eqs (26) and (27), for every $l \leq 0$ and $m \geq 0$. At $z = S_n(x)$, with $1 \leq n \leq N - 1$, eqs (29) and (32) are satisfied for every $m > 0$, and eqs (30) and (31), for every $m \geq 0$, though here, the sums in eqs (29) and (32) extend over the indices $l < 0$, and the sums in eqs (30) and (31) over the indices $l \leq 0$. Now, we multiply eqs (29) and (32) by $\sin(k_{xi}x)$ for every i between $-L$ and -1 and eqs (30) and (31) by $\cos(k_{xi}x)$ for every i between $-L$ and 0, and then we integrate x between $-\lambda_x/2$ and $\lambda_x/2$. Once again, we obtain systems of linear equations that can be solved independently for every m.

2.3 Model extension

The studied area is located between $x_{\min}$ and $x_{\max}$ such that $x_{\max} - x_{\min} = L_x$, and $y_{\min}$ and $y_{\max}$ such that $y_{\max} - y_{\min} = L_y$. Since, in general, $S_n(x_{\min})$ is different from $S_n(x_{\max})$, it is not possible to obtain a periodic function of x simply by extending S_n to the left and to the right as the constant values $S_n(x_{\min})$ and $S_n(x_{\max})$, respectively. Because of this, we instead centre the model at $x = \lambda_x/4$, and assume that

$$S_n(x) = \begin{cases} S_n(x_{\min}) & \text{if } 0 \leq x \leq x_{\min} \\ S_n(x_{\max}) & \text{if } x_{\max} \leq x \leq \lambda_x/2 \\ S_n(-x) & \text{if } -\lambda_x/2 \leq x \leq 0 \end{cases} \tag{32}$$

with $x_{\min} = \lambda_x/4 - L_x/2$ and $x_{\max} = \lambda_x/4 + L_x/2$. It is important to note that this extension of the interfaces does not impose any restriction on the type of functions $S_n(x)$ that can be considered inside the studied area. Furthermore, assuming that S_n is an even function of x greatly simplifies the treatment for reasons that are explained later in this section.

To calculate the coefficients B^0_{lm} and D^0_{lm}, we must select convenient extensions of $H_x^{(\mathrm{ext})}$ and $H_y^{(\mathrm{ext})}$ at $z = 0$. This is a more complex problem than the extension of the boundaries $S_n(x)$. First, we show how we extend these components, for periods such that the quasi-stationary approximation is valid in the air. In this approximation,

$$\bar{\nabla} \times \bar{H}_0 = \bar{\nabla} \times \bar{H}^{(\mathrm{ext})} = \bar{\nabla} \times \bar{H}^{(\mathrm{ind})} = 0, \tag{33}$$

where $\bar{H}^{(\mathrm{ind})}$ is the induced magnetic field. Then,

$$\partial_x H_y^{(\mathrm{ext})} - \partial_y H_x^{(\mathrm{ext})} = 0. \tag{34}$$

We are modelling the response to an external field that in a certain region is 3-D; there $\partial_x H_y^{(\mathrm{ext})}$ and $\partial_y H_x^{(\mathrm{ext})}$ are not null. We select the area to be studied such that it completely contains this region and assume that outside there $\partial_x H_y^{(\mathrm{ext})}$ and $\partial_y H_x^{(\mathrm{ext})}$ are null (this means that $H_x^{(\mathrm{ext})}$ does not depend on y and $H_y^{(\mathrm{ext})}$ does not depend on x). Then, at the surface of the earth, $H_y^{(\mathrm{ext})}$ must be constant at the borders of the studied area that correspond to $y = y_{\min}$ or $y = y_{\max}$, while $H_x^{(\mathrm{ext})}$ must be constant at the borders $x = x_{\min}$ and $x = x_{\max}$. In general, $H_x^{(\mathrm{ext})}$, which is a function of x, and $H_y^{(\mathrm{ext})}$, which is a constant, are different at the borders $y = y_{\min}$ and $y = y_{\max}$. Analogously, $H_x^{(\mathrm{ext})}$, which in this case is a constant, and $H_y^{(\mathrm{ext})}$, a function of y, are also different at the borders $x = x_{\min}$ and $x = x_{\max}$. Considering this, we centre the model at $(x, y) = (\lambda_x/2, \lambda_y/2)$, and extend these components to the area $0 \leq x \leq \lambda_x/2$, $0 \leq y \leq \lambda_y/2$, as follows:

$$H_x^{(\mathrm{ext})}(x, y, 0, \omega) = \begin{cases} H_x^{(\mathrm{ext})}(x, y_{\min}, 0, \omega) & \text{if } x_{\min} \leq x \leq x_{\max},\ 0 \leq y \leq y_{\min} \\ H_x^{(\mathrm{ext})}(x, y_{\max}, 0, \omega) & \text{if } x_{\min} \leq x \leq x_{\max},\ y_{\max} \leq y \leq \lambda_y/2 \\ H_x^{(\mathrm{ext})}(x_{\min}, y_{\min}, 0, \omega) = H_x^{(\mathrm{ext})}(x_{\min}, y_{\max}, 0, \omega) & \text{if } 0 \leq x \leq x_{\min},\ 0 \leq y \leq \lambda_y/2 \\ H_x^{(\mathrm{ext})}(x_{\max}, y_{\min}, 0, \omega) = H_x^{(\mathrm{ext})}(x_{\max}, y_{\max}, 0, \omega) & \text{if } x_{\max} \leq x \leq \lambda_x/2,\ 0 \leq y \leq \lambda_y/2 \end{cases} \tag{35}$$

$$H_y^{(\mathrm{ext})}(x, y, 0, \omega) = \begin{cases} H_y^{(\mathrm{ext})}(x_{\min}, y, 0, \omega) & \text{if } 0 \leq x \leq x_{\min},\ y_{\min} \leq y \leq y_{\max} \\ H_y^{(\mathrm{ext})}(x_{\max}, y, 0, \omega) & \text{if } x_{\max} \leq x \leq \lambda_x/2,\ y_{\min} \leq y \leq y_{\max} \\ H_y^{(\mathrm{ext})}(x_{\min}, y_{\min}, 0, \omega) = H_x^{(\mathrm{ext})}(x_{\max}, y_{\min}, 0, \omega) & \text{if } 0 \leq x \leq \lambda_x/2,\ 0 \leq y \leq y_{\min} \\ H_y^{(\mathrm{ext})}(x_{\min}, y_{\max}, 0, \omega) = H_x^{(\mathrm{ext})}(x_{\max}, y_{\max}, 0, \omega) & \text{if } 0 \leq x \leq \lambda_x/2 \\ y_{\max} \leq y \leq \lambda_y/2. \end{cases} \tag{36}$$

The simplest form to extend these components to the whole area $-\lambda_x/2 \le x \le \lambda_x/2, -\lambda_y/2 \le y \le \lambda_y/2$, considering that they usually are not null at the coordinate axes, would be to assume that the extended $\bar{H}^{(\mathrm{ext})}$ is such that $H_x^{(\mathrm{ext})}$ and $H_y^{(\mathrm{ext})}$ are even functions of x and y. As this is not compatible with eq. (35), we instead suppose that each one is the sum of both an even and an odd function of x and y. This corresponds to assuming that

$$\bar{H}^{(\mathrm{ext})} = \bar{H}^{(\mathrm{ext1})} + \bar{H}^{(\mathrm{ext2})}, \tag{37}$$

where $\bar{H}^{(\mathrm{ext1})}$ and $\bar{H}^{(\mathrm{ext2})}$ are the fields defined by eqs (15)–(17) and (18)–(20), respectively. We show next that this assumption unequivocally defines the extensions of $H_x^{(\mathrm{ext})}$ and $H_y^{(\mathrm{ext})}$ to the area $-\lambda_x/2 \le x \le \lambda_x/2, -\lambda_y/2 \le y \le \lambda_y/2$. The selected extension is advantageous because, as we have formerly pointed out, $\bar{H}^{(\mathrm{ext1})}$ and $\bar{H}^{(\mathrm{ext2})}$ give uncoupled responses when the boundaries S_n are even functions of x, and does not restrict the fields $\bar{H}^{(\mathrm{ext})}$ that can be considered in the studied area.

For the extended fields in the air, given by eqs (5)–(10) with $n = 0$, the quasi-stationary approximation corresponds to taking the limits $\gamma_0 \approx 0$ and $R_{00}^0 z \ll 1$. Then,

$$A_{00}^0 = B_{00}^0 \tag{38}$$

$$C_{00}^0 = D_{00}^0 \tag{39}$$

$$A_{0m}^0 = B_{0m}^0 = 0 \quad \text{if } m \neq 0 \tag{40}$$

$$C_{l0}^0 = D_{l0}^0 = 0 \quad \text{if } l \neq 0 \tag{41}$$

$$k_{ym} A_{lm}^0 = k_{xl} C_{lm}^0 \quad \text{if } l \neq 0 \text{ and } m \neq 0 \tag{42}$$

$$k_{ym} B_{lm}^0 = k_{xl} D_{lm}^0 \quad \text{if } l \neq 0 \text{ and } m \neq 0 \tag{43}$$

because, the electric field must not diverge. This hypothesis is stronger than eq. (34) and ensures its validity. Using eq. (34) alone, relations (41)–(44) could also be obtained but A_{00}^0 and C_{00}^0 could not be determined. Replacing relations (41)–(44) into eqs (15)–(20), we obtain that

$$H_x^{(\mathrm{ext1})}(x, y, z, \omega) = B_{00}^{(0)}(\omega) + \sum_{l>0, m\le 0} B_{lm}^{(0)}(\omega) \exp[-k_{rlm} S_n(x)] \cos(k_l x) \cos(k_m y) \tag{44}$$

$$H_y^{(\mathrm{ext1})}(x, y, z, \omega) = -\sum_{l>0, m<0} \frac{k_{ym}}{k_{xl}} B_{lm}^{(0)}(\omega) \exp[-k_{rlm} S_n(x)] \sin(k_l x) \sin(k_m y) \tag{45}$$

$$H_z^{(\mathrm{ext1})}(x, y, z, \omega) = -\sum_{l>0, m\le 0} \frac{k_{rlm}}{k_{xl}} B_{lm}^{(0)}(\omega) \exp[-k_{rlm} S_n(x)] \sin(k_l x) \cos(k_m y) \tag{46}$$

$$H_x^{(\mathrm{ext2})}(x, y, z, \omega) = -\sum_{l<0, m>0} \frac{k_{xl}}{k_{ym}} D_{lm}^{(0)}(\omega) \exp[-k_{rlm} S_n(x)] \sin(k_l x) \sin(k_m y) \tag{47}$$

$$H_y^{(\mathrm{ext2})}(x, y, z, \omega) = D_{00}^{(0)}(\omega) + \sum_{l\le 0, m>0} D_{lm}^{(0)}(\omega) \exp[-k_{rlm} S_n(x)] \cos(k_l x) \cos(k_m y) \tag{48}$$

$$H_z^{(\mathrm{ext2})}(x, y, z, \omega) = -\sum_{l\le 0, m>0} \frac{k_{rlm}}{k_{ym}} D_{lm}^{(0)}(\omega) \exp[-k_{rlm} S_n(x)] \cos(k_l x) \sin(k_m y), \tag{49}$$

where $k_{rlm} = \sqrt{k_{xl}^2 + k_{ym}^2}$. So, in this approximation, $\bar{H}^{(\mathrm{ext1})}$ is determined only by the coefficients B_{00}^0 and B_{lm}^0 with $l > 0$ and $m \le 0$ or by the function $H_x^{(\mathrm{ext1})}(x, y, 0, \omega)$, and $\bar{H}^{(\mathrm{ext2})}$ only by D_{00}^0 and D_{lm}^0 with $l \le 0$ and $m > 0$ or by $H_y^{(\mathrm{ext2})}(x, y, 0, \omega)$. Then, considering eq. (38), $\bar{H}^{(\mathrm{ext})}$ at $z = 0$, is given by

$$\begin{aligned} H_x^{(\mathrm{ext})}(x, y, 0, \omega) = {} & B_{00}^{(0)}(\omega) + \sum_{l>0, m\le 0} B_{lm}^{(0)}(\omega) \cos(k_l x) \cos(k_m y) \\ & - \sum_{l<0, m>0} \frac{k_{xl}}{k_{ym}} D_{lm}^{(0)}(\omega) \sin(k_l x) \sin(k_m y) \end{aligned} \tag{50}$$

$$\begin{aligned} H_y^{(\mathrm{ext})}(x, y, 0, \omega) = {} & -\sum_{l>0, m<0} \frac{k_{ym}}{k_{xl}} B_{lm}^{(0)}(\omega) \sin(k_l x) \sin(k_m y) + D_{00}^{(0)}(\omega) \\ & + \sum_{l\le 0, m>0} D_{lm}^{(0)}(\omega) \cos(k_l x) \cos(k_m y) \end{aligned} \tag{51}$$

$$\begin{aligned} H_z^{(\mathrm{ext})}(x, y, 0, \omega) = {} & -\sum_{l>0, m\le 0} \frac{k_{rlm}}{k_{xl}} B_{lm}^{(0)}(\omega) \sin(k_l x) \cos(k_m y) \\ & - \sum_{l\le 0, m>0} \frac{k_{rlm}}{k_{ym}} D_{lm}^{(0)}(\omega) \cos(k_l x) \sin(k_m y). \end{aligned} \tag{52}$$

Multiplying $H_x^{(\mathrm{ext})}(x, y, 0, \omega)$ by $\cos(k_{xi}x)\cos(k_{yj}y)$, for $(i, j) = (0, 0)$ and for every (i, j) with $0 < i \leq L$ and $-L \leq j \leq 0$, and $H_y^{(\mathrm{ext})}(x, y, 0, \omega)$ by $\cos(k_{xi}x)\cos(k_{yj}y)$, for $(i, j) = (0, 0)$ and for every (i, j) with $-L \leq i \leq 0$ and $0 < j \leq L$, and then integrating x and y over the area $0 \leq x \leq \lambda_x/2$, $0 \leq y \leq \lambda_y/2$, we obtain a system of $2[L(L+1)+1]$ linear equations that allows us to calculate the coefficients.

For periods such that the problem is not quasi-stationary, the restrictions imposed by eqs (35) and (41)–(44) are not present. Then, we simply extend $H_x^{(\mathrm{ext})}$ and $H_y^{(\mathrm{ext})}$ to the area $0 \leq x \leq \lambda_x/2$, $0 \leq y \leq \lambda_y/2$, as follows:

$$H_\tau^{(\mathrm{ext})}(x, y, 0, \omega) = \begin{cases} H_\tau^{(\mathrm{ext})}(x, y_{\min}, 0, \omega) & \text{if } x_{\min} \leq x \leq x_{\max},\ 0 \leq y \leq y_{\min} \\ H_\tau^{(\mathrm{ext})}(x, y_{\max}, 0, \omega) & \text{if } x_{\min} \leq x \leq x_{\max},\ y_{\max} \leq y \leq \lambda_y/2 \\ H_\tau^{(\mathrm{ext})}(x_{\min}, y, 0, \omega) & \text{if } 0 \leq x \leq x_{\min},\ y_{\min} \leq y \leq y_{\max} \\ H_\tau^{(\mathrm{ext})}(x_{\max}, y, 0, \omega) & \text{if } x_{\max} \leq x \leq \lambda_x/2,\ y_{\min} \leq y \leq y_{\max} \\ H_\tau^{(\mathrm{ext})}(x_{\min}, y_{\min}, 0, \omega) & \text{if } 0 \leq x \leq x_{\min},\ 0 \leq y \leq y_{\min} \\ H_\tau^{(\mathrm{ext})}(x_{\min}, y_{\max}, 0, \omega) & \text{if } 0 \leq x \leq x_{\min},\ y_{\max} \leq y \leq \lambda_y/2 \\ H_\tau^{(\mathrm{ext})}(x_{\max}, y_{\min}, 0, \omega) & \text{if } x_{\max} \leq x \leq \lambda_x/2,\ 0 \leq y \leq y_{\min} \\ H_\tau^{(\mathrm{ext})}(x_{\max}, y_{\max}, 0, \omega) & \text{if } x_{\max} \leq x \leq \lambda_x/2,\ y_{\max} \leq y \leq \lambda_y/2, \end{cases} \tag{53}$$

where τ denotes the x or y components of $\bar{H}^{(\mathrm{ext})}$, and assume, without lose of generality, that both components are even functions of x and y. This condition is satisfied when $\bar{H}^{(\mathrm{ext})}$ obeys eq. (38), and the fields $\bar{H}^{(\mathrm{ext1})}$ and $\bar{H}^{(\mathrm{ext2})}$ are such that the coefficients D_{lm}^0 with >0 and $m < 0$ in eqs (15)–(17), and the coefficients B_{lm}^0 with $l < 0$ and >0 in eqs (18)–(20), are null. Once more, the responses to these fields are uncoupled. In this case, to calculate the no null coefficients, B_{lm}^0 with $l \geq 0$ and $m \leq 0$, and D_{lm}^0 with $l \leq 0$ and $m \geq 0$, we multiply $H_x^{(\mathrm{ext})}(x, y, 0, \omega)$ by $\cos(k_{xi}x)\cos(k_{yj}y)$, for every (i, j) with $0 \leq i \leq L$ and $-L \leq j \leq 0$, and $H_y^{(\mathrm{ext})}(x, y, 0, \omega)$ by $\cos(k_{xi}x)\cos(k_{yj}y)$, for every (i, j) with $L \leq i \leq 0$ and $0 \leq j \leq L$, and then we integrate these functions in x and y over the area $-\lambda_x/2 \leq x \leq \lambda_x/2$, $-\lambda_y/2 \leq y \leq \lambda_y/2$, obtaining a system of $2(L+1)^2$ linear equations.

3 NON-UNIFORM SOURCE EFFECTS: COMPARISON WITH THE MAGNETOTELLURIC CASE

For the range of periods involved in MT soundings, the quasi-stationary approximation is valid in the air, and also inside the earth, for the conductivities usually found. In this approximation $\gamma_0 \approx 0$, $R_{00}^0 z \ll 1$ and $\omega\varepsilon_n \ll \sigma_n$ for $1 \leq n \leq N$. Furthermore, the external field is assumed to be horizontal and spatially uniform. This case corresponds to having only the coefficients $B_{00}^{(0)}$ in eqs (45)–(47), and $D_{00}^{(0)}$ in eqs (48)–(50), different from zero. Hence, for each frequency, the impedance tensor $\bar{\bar{Z}}$ and the tipper $\bar{T}$, which are, respectively, defined as (see, for example, Weaver 1994):

$$\begin{bmatrix} E_x \\ E_y \end{bmatrix}(x, y, 0, \omega) = \begin{bmatrix} Z_{xx} & Z_{xy} \\ Z_{yx} & Z_{yy} \end{bmatrix}(x, y, \omega) \begin{bmatrix} H_x \\ H_y \end{bmatrix}(x, y, 0, \omega) \tag{54}$$

$$H_z(x, y, 0^+, \omega) = \begin{bmatrix} T_x & T_y \end{bmatrix}(x, y, \omega) \begin{bmatrix} H_x \\ H_y \end{bmatrix}(x, y, 0, \omega) \tag{55}$$

(where 0^+ means just below the air–earth surface), depend on the subsurface structure but not on the external field. As it is well known, for 2-D structures, there exist two uncoupled modes of propagation, the transverse electric, TE, and the transverse magnetic,TM, modes. If the strike direction is y, $\bar{H}^{(\mathrm{ext1})}$ and $\bar{H}^{(\mathrm{ext2})}$ generate, respectively, the TE and TM modes. Z_{xx}, Z_{yy} and T_y are null; $Z_{yx} = Z_{\mathrm{TE}}$ and $T_x = T_{\mathrm{TE}}$ are the TE mode responses, and $Z_{xy} = Z_{\mathrm{TM}}$ is the TM response.

For a spatially non-uniform source, there are other coefficients than $B_{00}^{(0)}$ in eqs (45)–(47), and $D_{00}^{(0)}$ in eqs (48)–(50), different from zero. Since the responses to these two fields are still uncoupled, and due to the validity of the superposition principle, each field component in eqs (5)–(10) is given by the sum of two terms, one depending only on the coefficients B_{00}^0 and B_{lm}^0 with $l > 0$ and $m \leq 0$ or on the function $H_x^{(\mathrm{ext1})}(x, y, 0, \omega)$, and the other depending only on D_{00}^0 and D_{lm}^0 with $l \leq 0$ and $m > 0$ or on $H_y^{(\mathrm{ext2})}(x, y, 0, \omega)$. Hence, naming the horizontal components of $\bar{H}$ and $\bar{E}$, $\bar{H}_{\mathrm{hor}}$ and $\bar{E}_{\mathrm{hor}}$, respectively, and defining $\bar{H}_{\mathrm{hor}}^{(\mathrm{ext})}$ as

$$\bar{H}_{\mathrm{hor}}^{(\mathrm{ext})}(x, y, 0, \omega) = H_x^{\mathrm{ext1}}(x, y, 0, \omega)\hat{x} + H_y^{\mathrm{ext2}}(x, y, 0, \omega)\hat{y} \tag{56}$$

the following relations can be written as

$$\bar{H}_{\mathrm{hor}}(x, y, 0, \omega) = \bar{\bar{\eta}}(x, y, \omega)\bar{H}_{\mathrm{hor}}^{(\mathrm{ext})}(x, y, 0, \omega) \tag{57}$$

$$H_z(x, y, 0, \omega) = \bar{\vartheta}(x, y, \omega)\bar{H}_{\mathrm{hor}}^{(\mathrm{ext})}(x, y, 0, \omega) \tag{58}$$

$$\bar{E}_{\mathrm{hor}}(x, y, 0, \omega) = \bar{\bar{\xi}}(x, y, \omega)\bar{H}_{\mathrm{hor}}^{(\mathrm{ext})}(x, y, 0, \omega), \tag{59}$$

where $\bar{\bar{\eta}}$ and $\bar{\bar{\xi}}$ are tensors of dimension (2×2), and $\bar{\vartheta}$ is a file vector of dimension two. η_{xx}, η_{yx}, ϑ_x, ξ_{xx} and ξ_{yx} depend on $H_x^{(\mathrm{ext1})}(x, y, 0, \omega)$, and η_{xy}, η_{yy}, ϑ_y, ξ_{xy} and ξ_{yy} depend on $H_y^{(\mathrm{ext2})}(x, y, 0, \omega)$. Then, $\bar{\bar{Z}}$ and $\bar{T}$ are given by

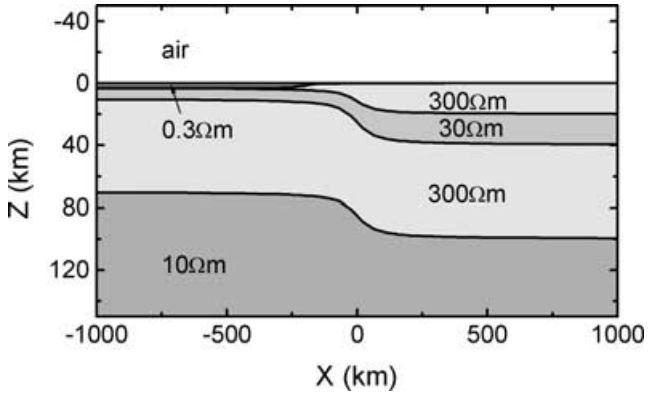

Figure 2. 2-D electrical model proposed to represent the kind of resistivity distribution that could be found at coastlines.

$$\bar{\bar{Z}}(x, y, \omega) = \bar{\bar{\xi}}(x, y, \omega)\bar{\bar{\eta}}^{-1}(x, y, \omega) \tag{60}$$

$$\bar{T}(x, y, \omega) = \bar{\vartheta}(x, y, \omega)\bar{\bar{\eta}}^{-1}(x, y, \omega). \tag{61}$$

When $\bar{H}^{(\mathrm{ext1})}$ is non-uniform and $\bar{H}^{(\mathrm{ext2})}$ is uniform, only Z_{xx}, Z_{yx} and T_x contain source effects. These magnitudes constitute generalizations of the MT TE responses. Conversely, when $\bar{H}^{(\mathrm{ext1})}$ is uniform and $\bar{H}^{(\mathrm{ext2})}$ is non-uniform, source effects are present only in Z_{xy}, Z_{yy} and T_y, which in this case are generalizations of the MT TM responses.

As has been stated previously, the uniform source hypothesis used for MT interpretation has proved to work well in a great number of studies, especially those carried out at mid latitudes, and for periods not exceeding 1000s, approximately. Nevertheless, at low or high latitudes, and for hourly or greater periods, this hypothesis usually fails, and then the electrical models obtained assuming 1-D external fields contain source distortions. In the following section we study how source distortions affect the responses at coastlines by comparison with the results obtained for 1-D sources.

4 APPLICATION: SOURCE EFFECTS AT COASTLINES

For this study we select a 2-D electrical model that can be considered representative of this kind of tectonic environment. This model is shown in Fig. 2. The upper layer corresponds to the ocean, the second one to the continental upper crust, the more conductive third one to the continental lower crust and to the oceanic crust, the fourth one to the lithospheric mantle and the deeper one to the beginning of the asthenosphere. We have analysed the responses of this structure to 1-D and different 2-D and 3-D, external fields, for a wide range of periods, arriving at the conclusion that source effects begin to be noticeable for periods greater than approximately 6 h and become larger as the period increases. Considering this and in order to not excessively increase the length of this paper, in this section we only present the responses obtained at a period of 24 h.

4.1 1-D, 2-D and 3-D $\bar{H}^{(\mathrm{ext1})}$—uniform $\bar{H}^{(\mathrm{ext2})}$

As we explained in the previous section, if $\bar{H}^{(\mathrm{ext2})}$ is 1-D, only the xx and yx components of $\bar{\bar{Z}}$(and the corresponding apparent resistivities ρ_{xx} and ρ_{yx}, and phases ϕ_{xx} and ϕ_{yx}) and T_x can contain source effects, which depend on the morphology of $\bar{H}^{(\mathrm{ext1})}$. In particular, if $\bar{H}^{(\mathrm{ext1})}$ is also 1-D, ρ_{xx} and ϕ_{xx} are null, and ρ_{yx}, ϕ_{yx} and T_x are the MT TE mode responses. In this case $\bar{H}^{(\mathrm{ext1})}$ is polarized in the x direction and has only one non-null coefficient: $B^{(0)}_{00}$.

The MT TE responses of the model shown in Fig. 2 are displayed in Fig. 3. ρ_{yx} and ϕ_{yx} exhibit low variation ranges, between 8 and 15 Ω m and 38° and 54°, respectively. The maximum magnitude of T_x is about 0.18.

Now, we consider two different 2-D external fields $\bar{H}^{(\mathrm{ext1})}$ with strike direction y, $\bar{H}^{(\mathrm{ext1})}$ 2D+ (shown in Figs 4a and b) and $\bar{H}^{(\mathrm{ext1})}$ 2-D− (shown in Figs 4c and d). The anomalous zones of both fields have characteristic widths similar to that of the equatorial electrojet (1000 km, approximately), and are centred just over the structure. In fact, $\bar{H}^{(\mathrm{ext1})}$ 2-D+ is a simplified representation of the field that would produce an equatorial electrojet oriented in the y direction. $\bar{H}^{(\mathrm{ext1})}$ 2-D− has a somewhat more complex spatial dependence; in particular, its x component is null at two values of x. For these fields, the non-null coefficients are only $B^{(0)}_{l0}$ for $l \geq 0$. From eqs (45)–(47), it is seen that they are necessarily polarized in the x–z plane. Both x components can be normalized to one outside the anomalous zones without affecting the responses. Fig. 5 shows the response of the proposed model to the field $\bar{H}^{(\mathrm{ext1})}$ 2-D+. Comparing with Fig. 3, the most remarkable fact is that ρ_{yx} is lower than in the former case, while ϕ_{yx} is greater, below the centre of the anomalous field. In contrast, ρ_{yx} is greater and ϕ_{yx} is lower, below both sides. The maximum value of the tipper is 0.77. Fig. 6 displays the response to the field 2-D−. The variations of ρ_{yx} and ϕ_{yx} are much greater than in the former cases. Note the presence of two narrow high-resistivity and low-phase zones. They are located just over the lines where $H^{(\mathrm{ext1})}_x$ is equal to zero. Along the left of these zones, tipper values are also much greater than those obtained for a 1-D source, reaching 14.

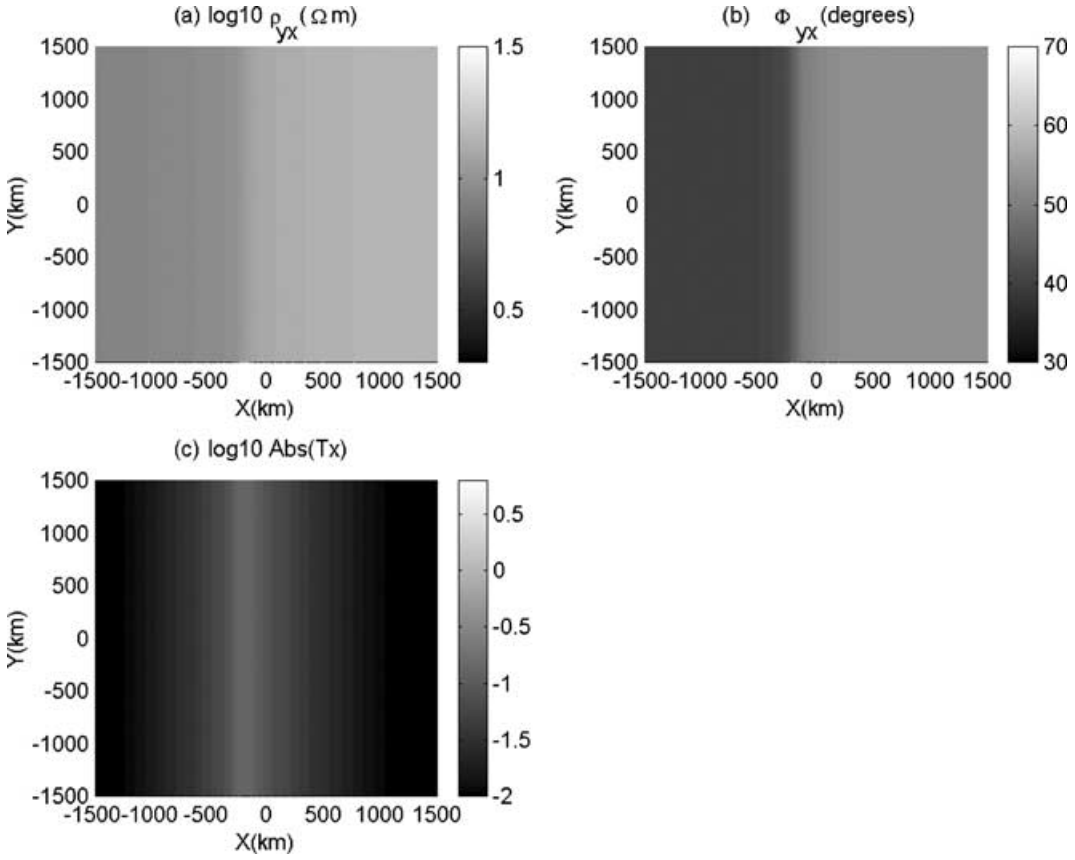

Figure 3. Response of the model shown in Fig. 2 to a spatially uniform inducing field polarized in the x direction (MT TE mode response), at a period of 24 h.

The spatial dependence of the external fields can be much more complex, for example, in zones where auroral electrojets are present. These fields can be 3-D and can have varied morphologies. As a first approximation to this kind of situation, we also selected two 3-D $\bar{H}^{(\mathrm{ext1})}$ fields, $\bar{H}^{(\mathrm{ext1})}$ 3-D+ (shown in Fig. 7) and $\bar{H}^{(\mathrm{ext1})}$3-D− (shown in Fig. 8). The anomalies of these fields have an areal extension of 1000 × 1000 km^2, and once again its x components are normalized to unity outside the anomalous zones. The response to the field $\bar{H}^{(\mathrm{ext1})}$ 3-D+, at a period of 24 h is shown in Fig. 9. In this case a dependence of the response on the y coordinate appears that is purely a 3-D source effect. ρ_{yx} and ϕ_{yx} variation ranges are similar to those obtained for the source $\bar{H}^{(\mathrm{ext1})}$ 2-D+, although maximum $|T_x|$ values are greater. Fig. 10 displays the response to the field $\bar{H}^{(\mathrm{ext1})}$ 3-D−. As in the response to the field $\bar{H}^{(\mathrm{ext1})}$ 2-D−, two zones of very high resistivity and tipper magnitude appear where the values of $H_x^{(\mathrm{ext1})}$ tend to zero. The difference is that in this case, these zones and those with lower values of ϕ_{yx} are not coincident. ϕ_{yx} has a wide variation range, almost between 0° and 90°. Comparing Fig. 3 to Figs 9 and 10, it is seen that the MT TE response of the 2-D structure is almost totally masked by 3-D source effects in the area located below the anomalies of the inducing fields.

4.2 Uniform $\bar{H}^{(\mathrm{ext1})}$—1-D and 3-D $\bar{H}^{(\mathrm{ext2})}$

When $\bar{H}^{(\mathrm{ext1})}$ is 1-D, source effects can only appear in ρ_{xy}, ρ_{yy}, ϕ_{xy}, ϕ_{yy} and T_y, and depend on the morphology of $\bar{H}^{(\mathrm{ext2})}$. If $\bar{H}^{(\mathrm{ext2})}$ is also 1-D, having only the coefficient $D_{00}^{(0)}$ different from 0, ρ_{yy}, ϕ_{yy} and T_y are null, and ρ_{xy} and ϕ_{xy} correspond to the MT TM mode response. In this case $\bar{H}^{(\mathrm{ext2})}$ is polarized in the y direction.

Fig. 11 shows the MT TM response of the proposed 2-D model. As expected, this response exhibits greater and more localized anomalies than the MT TE mode response (Fig. 3). A great part of these anomalies correspond to coastal effects.

A 2-D $\bar{H}^{(\mathrm{ext2})}$ field with strike direction y would correspond to only having $D^{(0)}{}_{l0}$ different from 0 for $l \leq 0$. Then, according to eqs (18)–(20), it might be polarized along the y axis. It is well known that it is not possible to have such a 2-D external field in quasi-stationary cases. This is corroborated here by eqs (48)–(50). So, in the following we consider directly the case of 3-D $\bar{H}^{(\mathrm{ext2})}$ fields.

We selected two $\bar{H}^{(\mathrm{ext2})}$ fields, $\bar{H}^{(\mathrm{ext2})}$ 3-D+ and $\bar{H}^{(\mathrm{ext2})}$ 3-D−, which are similar to the fields $\bar{H}^{(\mathrm{ext1})}$ 3-D+ and $\bar{H}^{(\mathrm{ext1})}$ 3-D− proposed previously, but rotated by 90° (Figs 12 and 13, respectively). Fig. 14 shows the response to $\bar{H}^{(\mathrm{ext2})}$ 3-D+. Comparing Fig. 14 with Fig. 11, a zone with lower resistivity and greater phase than for the uniform source is clearly observed, just below the central anomaly of the 3-D field. Additionally, values of $|T_y|$ different from 0 are found. They can reach up to 7. Fig. 15 plots the response to $\bar{H}^{(\mathrm{ext2})}$ 3-D−. Once more, two narrow zones of very high resistivity and tipper values can be identified that in this case, coincide with the zones where $H_y^{(\mathrm{ext2})}$ tends to zero. For both external fields, $\bar{H}^{(\mathrm{ext2})}$ 3-D+ and $\bar{H}^{(\mathrm{ext2})}$ 3-D−, source distortions of ϕ_{xy} are as important as the distortions observed in ϕ_{yx} for the

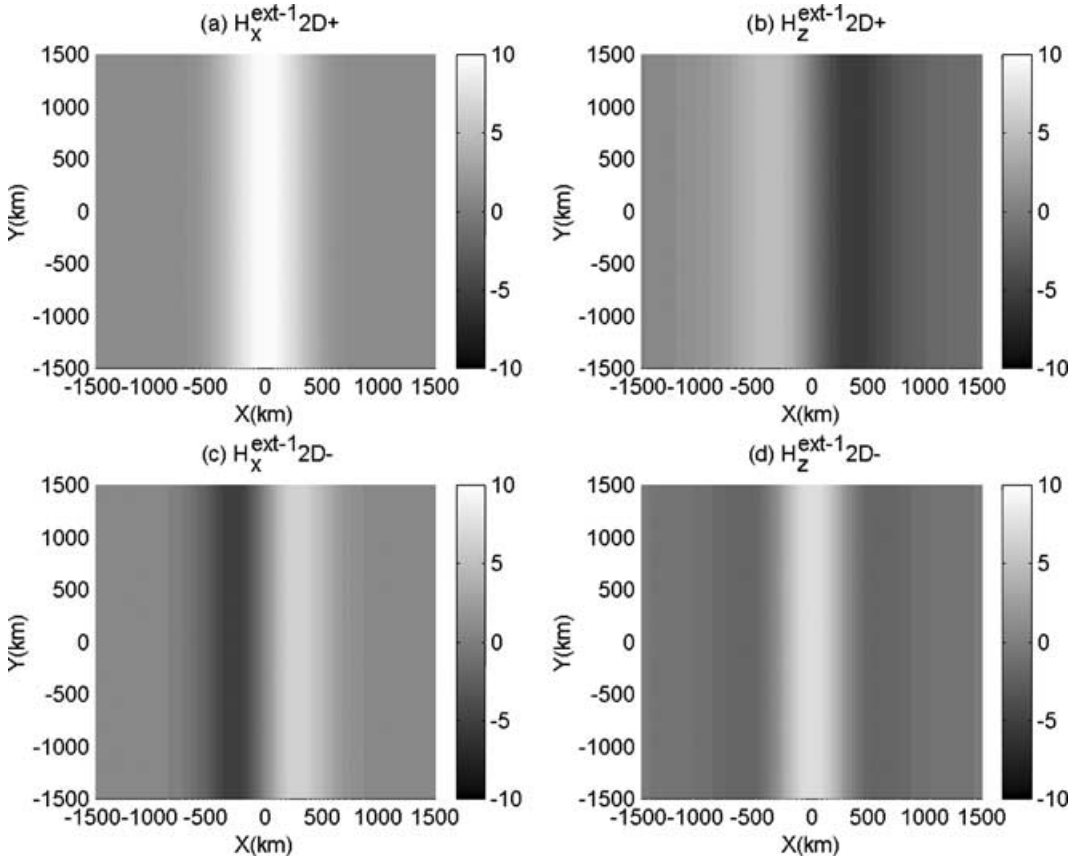

Figure 4. Spatial dependence of the 2-D inducing magnetic fields considered, $\bar{H}^{(\mathrm{ext1})}$ 2-D+ and $\bar{H}^{(\mathrm{ext1})}$ 2-D−, at the Earth's surface. These fields have a harmonic time dependence with a period of 24 h. $H_x^{(\mathrm{ext1})}$ 2-D+ is an even function of x, and $H_x^{(\mathrm{ext1})}$ 2-D− is an odd function plus a constant. The anomalies have a width of about 1000 km, similar to that of the equatorial electrojet, and the value of the x components outside the anomalous zone has been normalized to 1.

fields $\bar{H}^{(\mathrm{ext1})}$ 3-D+ and $\bar{H}^{(\mathrm{ext1})}$ 3-D−. Source distortions of ρ_{xy} are relatively less important, and a great part of the MT TM response can still be appreciated.

5 CONCLUSIONS

In the present work, we present a method for the calculation of the electromagnetic response of 2-D multilayered earth structures having smooth, irregular boundaries, to arbitrary, non-uniform, 2-D or 3-D external fields. This method is based on the application of a Rayleigh–Fourier technique and was obtained by extending previous MT 2-D and 3-D Rayleigh–Fourier modelling codes.

Applying this method, we made a theoretical investigation of the magnitude and characteristics of MT source effects at coastlines. We selected a 2-D electrical model with strike direction y, which can be considered representative of this kind of tectonic region, and we calculated the response of this model, $\bar{\bar{Z}}$ and $\bar{T}$, at the Earth's surface to different spatially non-uniform 2-D and 3-D inducing fields, over a broad range of periods. We evaluated source effects by comparing these responses with those obtained for 1-D sources. The spatial dependence of the fields produced, for example, by equatorial and auroral electrojets, as well as the source effects produced by these fields on 2-D structures, can be highly complex. As a first approximation to this problem, and in order to obtain general conclusions concerning the main and more basic characteristics of these effects, we selected geometries of the external fields, which are relatively simple, but contain several of the more important and typical features found in practice. We let the spatial dependence of each selected source be fixed and varied only its period. Nevertheless, it must be taken into account that the spatial dependence of actual sources depends on the period. In all of the studied cases, we found that source effects begin to be detectable for periods greater than approximately 6 h, and increase with period. At a period of 24 h, they are very important, as has been shown in the previous section. For each particular source, the zones in which the different components of the response are enhanced or decreased, do not change with period.

As is well known, for uniform sources and 2-D structures with strike direction y, Z_{yx} and T_x are the MT TE mode responses and Z_{xy} is the MT TM mode response, while Z_{xx}, Z_{yy} and T_y are null. One relevant theoretical result of this work is that the 3-D non-uniform inducing field could be separated into two contributions, one that produces source effects only in Z_{xx}, Z_{yx} and T_x and another that produces source effects only in Z_{yy}, Z_{xy} and T_y. Then, these magnitudes can be thought of as generalized TE and TM responses, respectively, although it is important to point out that they do not correspond strictly to TE and TM modes of propagation.

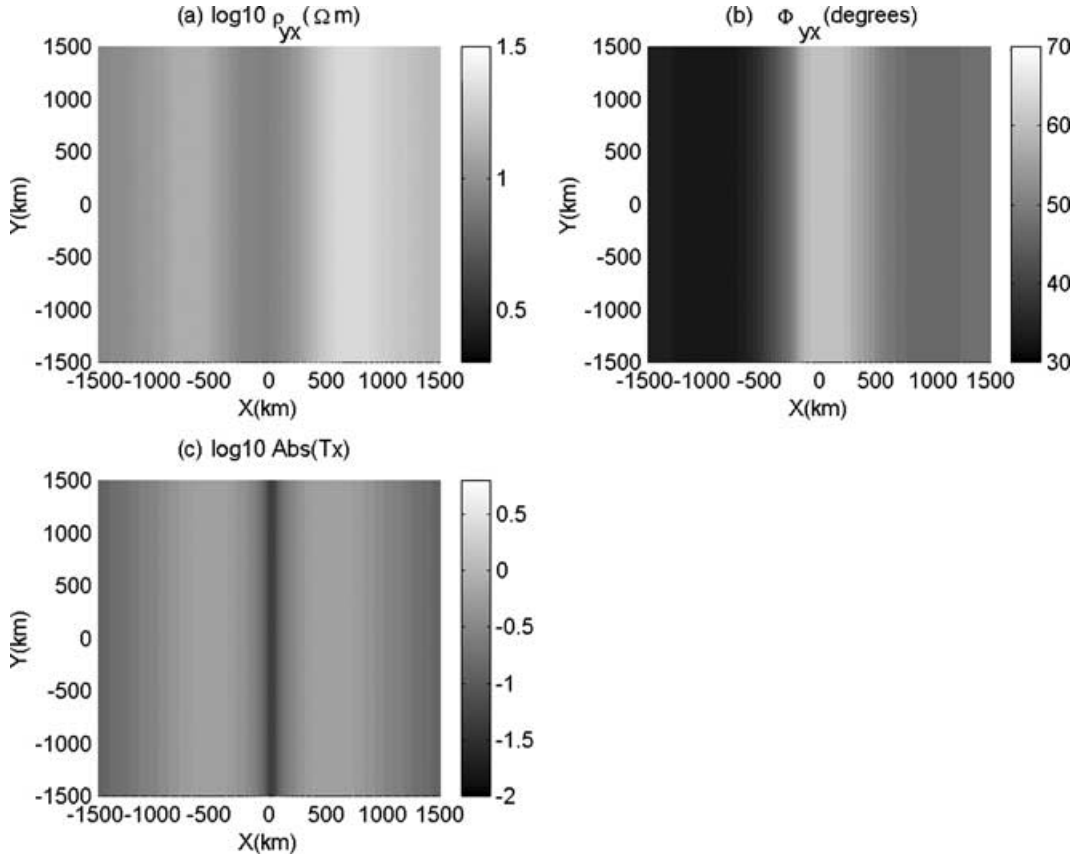

Figure 5. Response to the external field $\tilde{H}^{(\mathrm{ext1})}$ 2-D+.

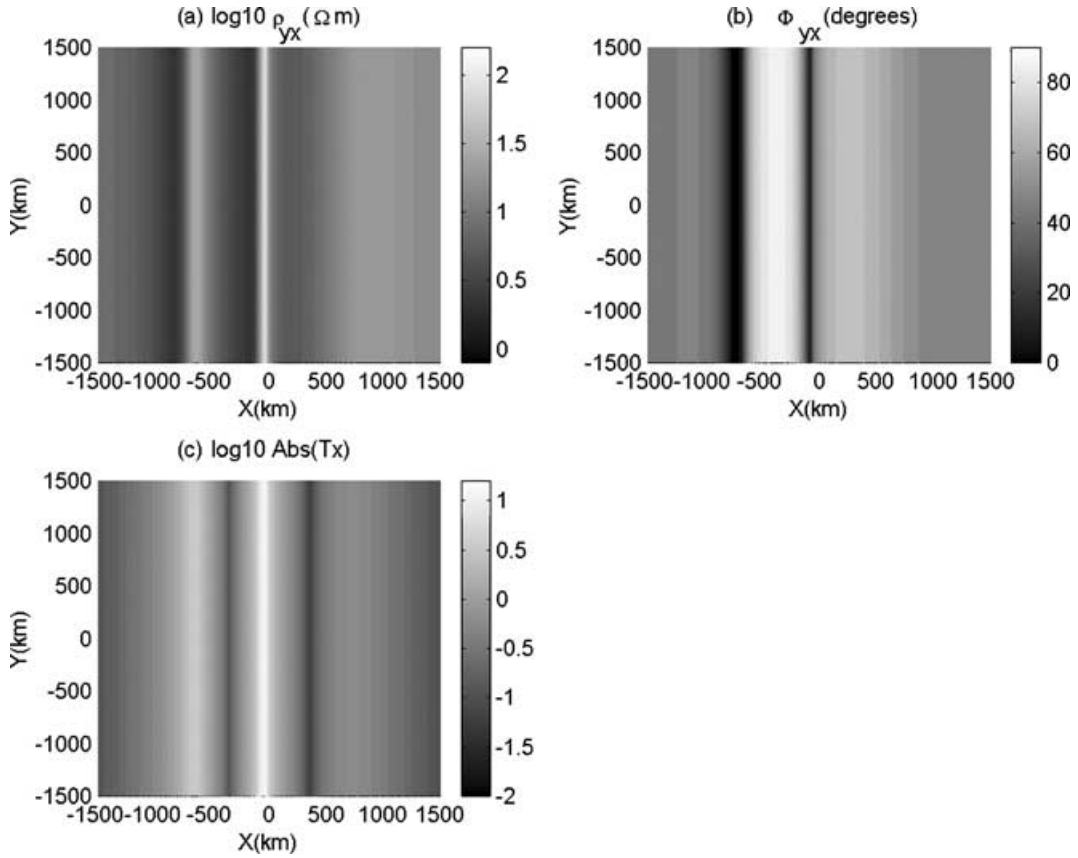

Figure 6. Response to the external field $\tilde{H}^{(\mathrm{ext1})}$ 2-D−.

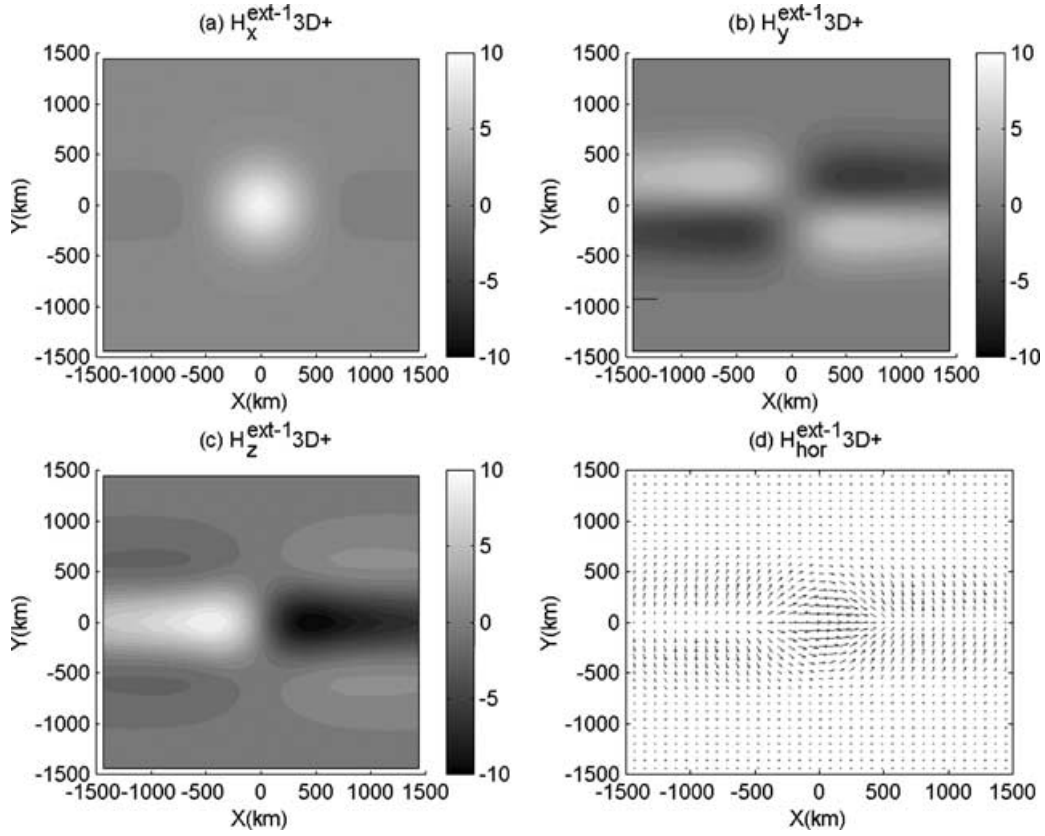

Figure 7. Spatial dependence of the first 3-D $\bar{H}^{(ext1)}$ inducing field considered, $\bar{H}^{(ext1)}$ 3-D+, at the Earth's surface. This field has a harmonic time dependence with a period of 24 h. The x component is an even function of x and y, and its value outside the anomalous zone has been normalized to 1.

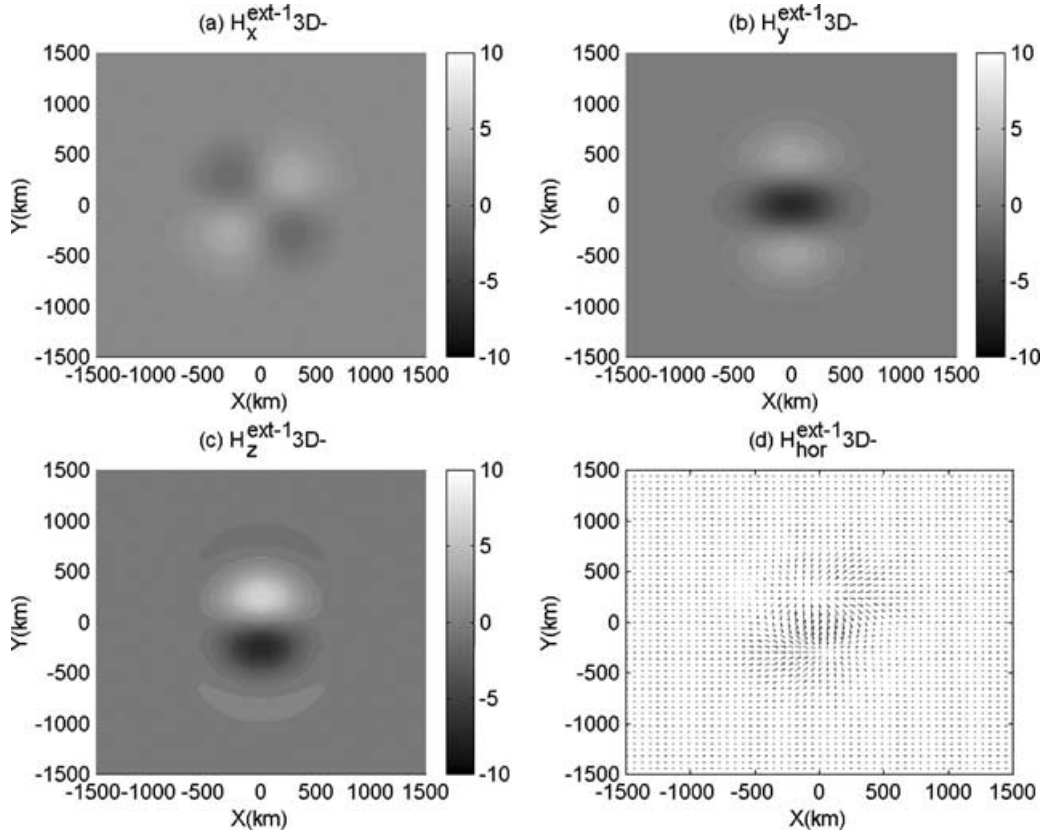

Figure 8. Spatial dependence of the second 3-D $\bar{H}^{(ext1)}$ inducing magnetic field considered, $\bar{H}^{(ext1)}$ 3-D−, at the Earth's surface. The x component is an odd function of x and y plus a constant, and its value outside the anomalous zone has been normalized to 1.

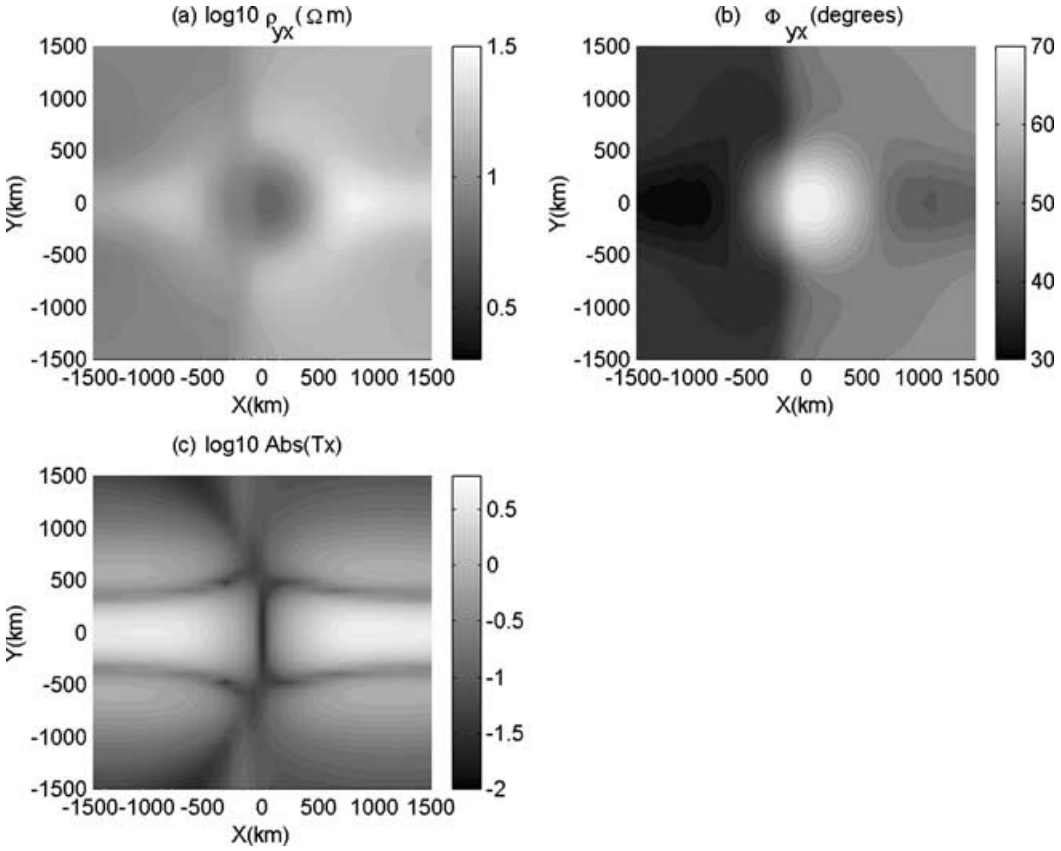

Figure 9. Response to the external field $\bar{H}^{(ext1)}$ 3-D+.

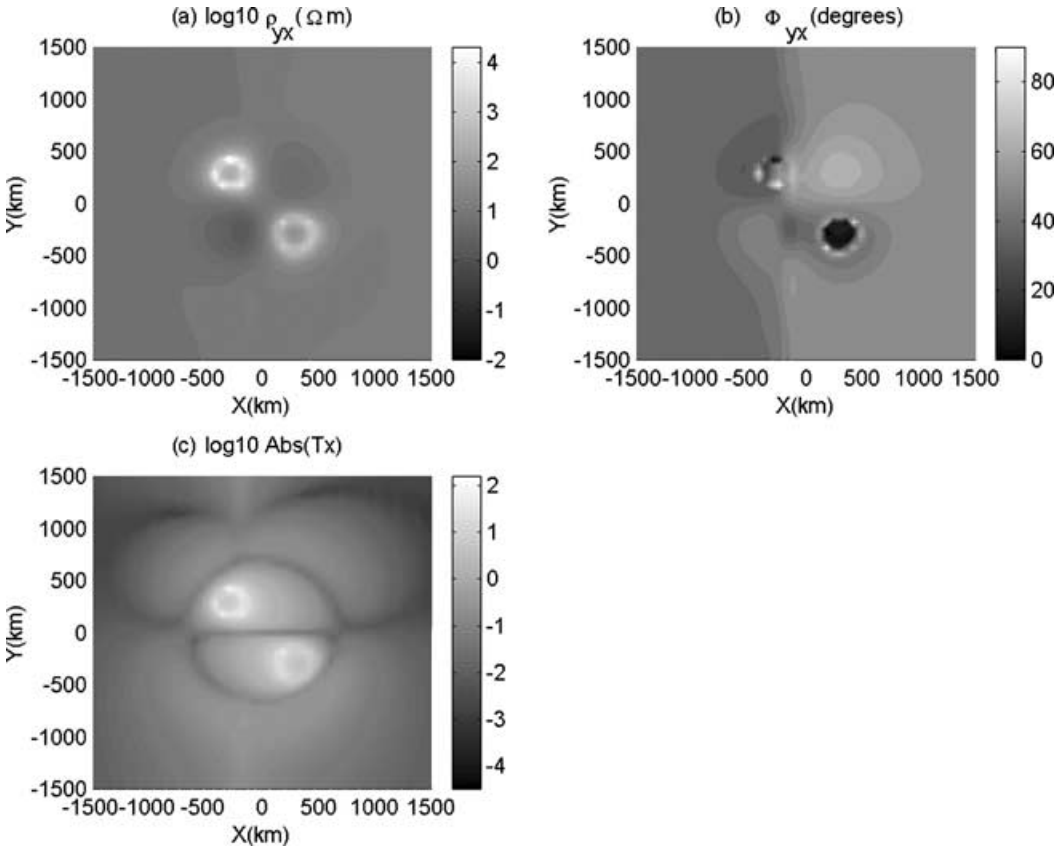

Figure 10. Response to the external field $\bar{H}^{(ext1)}$ 3-D−.

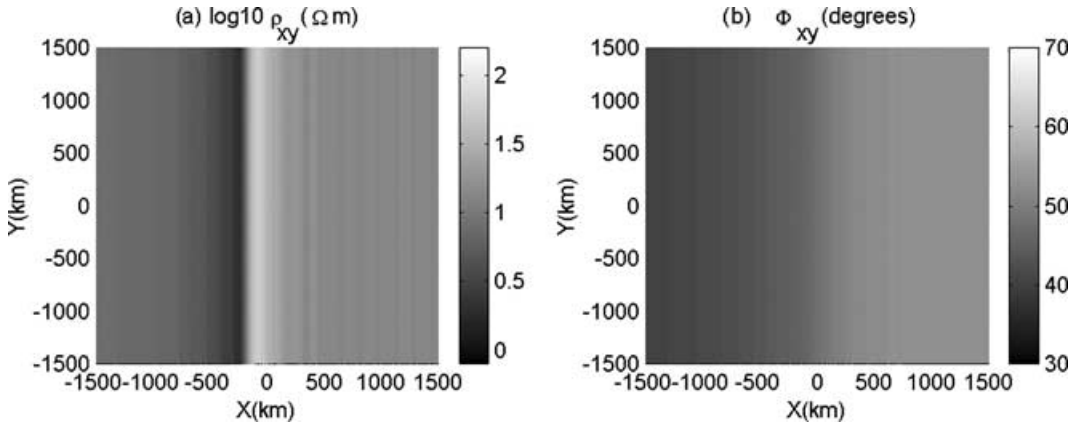

Figure 11. Response to a spatially uniform inducing field polarized in the y direction (MT TM mode response), at the period 24 h. T_y is null.

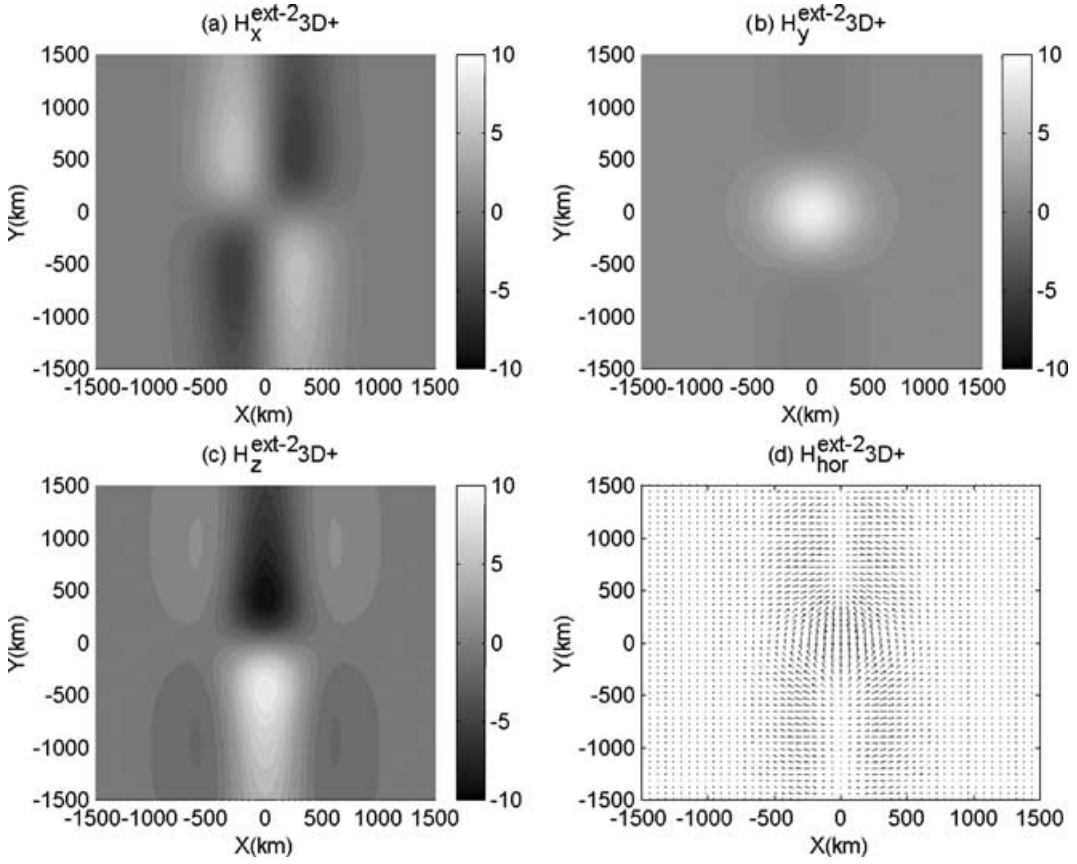

Figure 12. Spatial dependence of the first 3-D $\bar{H}^{(\mathrm{ext2})}$ inducing field considered, $\bar{H}^{(\mathrm{ext2})}$ 3-D+, at the Earth's surface. This field has a harmonic time dependence with period 24 h. The y component is an even function of x and y, and its value outside the anomalous zone has been normalized to 1.

First, we considered external fields $\bar{H}^{(\mathrm{ext1})}$ that produce source effects on the TE responses. The fields considered are 1-D far from the structure and near the structure have 2-D or 3-D anomalies. We found that when the anomaly of $H_x^{(\mathrm{ext1})}$ is an even function of x ($\bar{H}^{(\mathrm{ext1})}$ 2-D+) or an even function of x and y ($\bar{H}^{(\mathrm{ext1})}$ 3-D+), which corresponds to an increase of this component over the structure, the values of ρ_{yx} are lower than those obtained for 1-D sources, below the centre of the anomaly, while they are greater towards both sides. ϕ_{yx} follows the inverse behaviour. Variation ranges of these magnitudes are similar in both cases. On the other hand, if $H_x^{(\mathrm{ext1})}$ is a constant plus an odd function of x ($\bar{H}^{(\mathrm{ext1})}$ 2-D−) or an odd function of x and y ($\bar{H}^{(\mathrm{ext1})}$ 3-D−), narrow zones of high resistivity and $|T_x|$ are observed, where $H_x^{(\mathrm{ext1})}$ tends to zero. There, the variation ranges of ρ_{yx} and $|T_x|$ are almost an order of magnitude greater than those obtained for a 1-D source. The lower values of ϕ_{yx} are also reached at these zones in the 2-D− case, but not in the 3-D− case. In both cases, ϕ_{yx} varies almost between 0° and 90°.

Next, we analysed source effects on the TM responses. We considered two fields, $\bar{H}^{(\mathrm{ext2})}$ 3-D+ and $\bar{H}^{(\mathrm{ext2})}$ 3-D−, which were obtained by rotating 90° $\bar{H}^{(\mathrm{ext1})}$ 3-D+ and $\bar{H}^{(\mathrm{ext1})}$ 3-D−, respectively. Then the anomaly of the y component of $\bar{H}^{(\mathrm{ext2})}$ 3-D+ is an even function of x

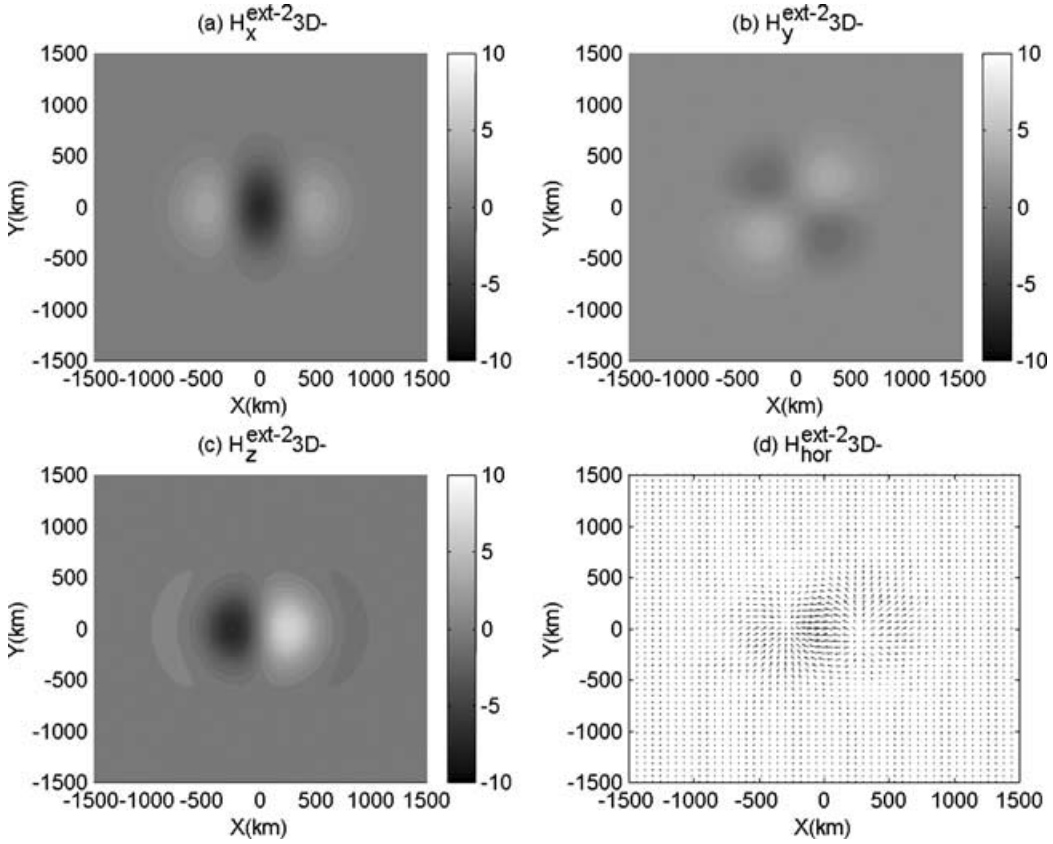

Figure 13. Spatial dependence of the second 3-D $\tilde{H}^{(ext2)}$ inducing magnetic field considered, $\tilde{H}^{(ext2)}$ 3-D−, at the Earth's surface. The *y* component is an odd function of *x* and *y* plus a constant, and its value outside the anomalous zone has been normalized to 1.

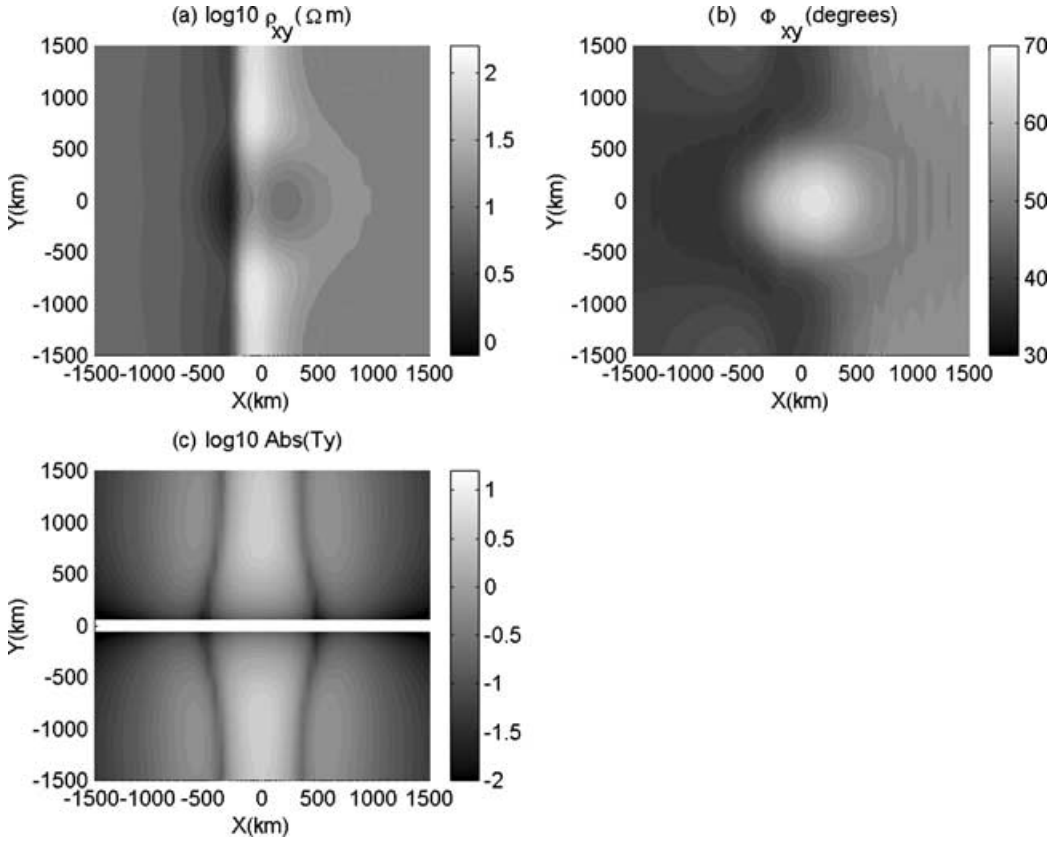

Figure 14. Response to the external field $\tilde{H}^{(ext2)}$ 3-D+.

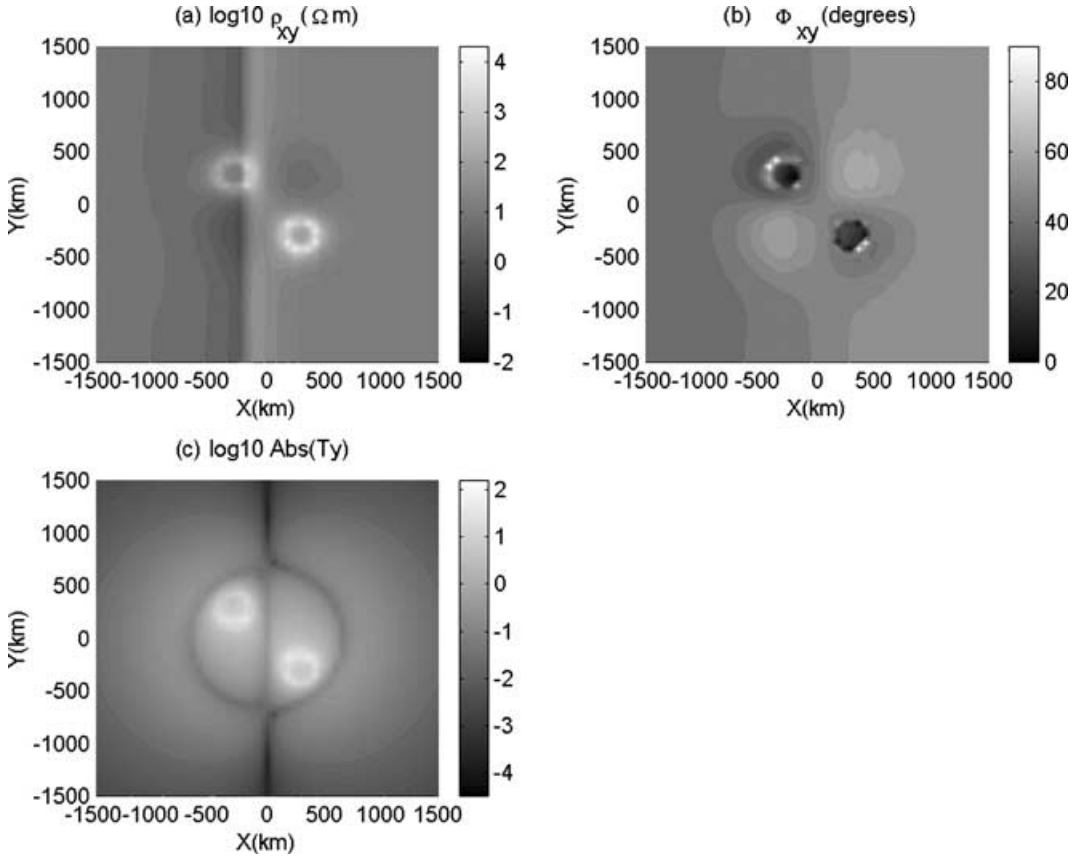

Figure 15. Response to the external field $\bar{H}^{(\mathrm{ext2})}$ 3-D−.

and y, while the anomaly of the y component of $\bar{H}^{(\mathrm{ext2})}$ 3-D− is an odd function of x and y plus a constant. For $\bar{H}^{(\mathrm{ext2})}$ 3-D+, similarly to the behaviour observed for $\bar{H}^{(\mathrm{ext1})}$ 2-D+ and 3-D+, ρ_{xy} is depressed and ϕ_{xy} is enhanced below the centre of the anomaly of this field. In addition, T_y is not null. The field $\bar{H}^{(\mathrm{ext2})}$ 3-D− produces narrow zones of extremely high resistivity and tipper.

We can conclude that at a period of 24 h, below the central part of the anomalies of all the $\bar{H}^{(\mathrm{ext1})}$ fields considered, the generalized TE responses are completely dominated by source effects and are very different from the MT TE mode response. Conversely, the source effects produced by the two fields $\bar{H}^{(\mathrm{ext2})}$ are more localized and relatively less important, such that a great part of the MT TM mode response can still be appreciated, even at this large period.

Although these results were obtained for a particular kind of 2-D structure, and for particular types of external fields, they provide some basic conclusions that could be extended to other analogous situations.

ACKNOWLEDGMENTS

This work was supported by the ANPCYT (Agencia Nacional de Promoción Científica y Tecnológica) and CONICET (Consejo Nacional de Investigaciones Científicas y Técnicas).

REFERENCES

Bahr, K. & Filloux, J.H., 1989. Local S_q responses from EMSLAB data, *J. geophys. Res.,* **95,** 14 195–14 200.

Boteler, D.H. & Pirjola, R., 1998. The complex-image method for calculating the magnetic and electric fields at the surface of the Earth by the auroral electrojet, *Geophys. J. Int.,* **132,** 31–40.

Cagniard, L., 1953. Basic theory of the magnetotelluric method of geophysical prospecting, *Geophysics,* **18,** 605–635.

Carrasquilla, A. & Rijo, L., 1998. Analysis of electrojet-distorted magnetotelluric sounding curves, *J. appl. Geophys.,* **40,** 187–204.

Dimitriev, V.I. & Berdichevsky, M.N., 1979. The fundamental model of magnetotelluric sounding, *Proc. IEEE,* **67,** 1033–1044.

Favetto, A., Martinelli, P. & Osella, A., 1997. Electrical and thermal anomalies in the Central Andean subduction zone, *Pure appl. Geophys.,* **149,** 391–404.

Gough, D.I., McKirdy, D.M., Woods, D.V. & Geiger, H., 1989. Conductive structures and tectonics beneath the EMSLAB land array, *J. geophys. Res.,* **94,** 14 099–14 110.

Häkkinen, L. & Pirjola, R., 1986. Calculation of electric and magnetic fields due to an electrojet current system above a layered earth, *Geophysica,* **22,** 31–44.

Korja, T. & the BEAR Working Group, 1998. BEAR. Baltic Electromagnetic Array Research, *Europrobe News,* **12,** 4–5.

Mareschal, M., 1981. Source effects an the interpretation of geomagnetic sounding data at sub-auroral latitudes, *Geophys. J. R. astr. Soc.,* **67,** 125–136.

Martinelli, P. & Osella, A., 1997. MT forward modeling of 3D anisotropic electrical conductivity structures using the Rayleigh–Fourier method, *J. Geomag. Geoelectr.,* **49,** 1499–1518.

Osella, A. & Martinelli, P., 1993. Magnetotelluric response of anisotropic 2-D structures, *Geophys. J. Int.,* **115,** 819–828.

Osella, A.M., Favetto, A. & Martinelli, P., 1993a. Sensitivity of the geomagnetic daily variations to 2-D structures, *Trends Geophys. Res.,* **2,** 141–155.

Osella, A.M., Favetto, A. & Martinelli, P., 1993b. Lateral heterogeneities in the upper and mid-mantle conductivity in Argentina, *Pure appl. Geophys.,* **141,** 139–156.

Osipova, I.L., Hjelt, S.E. & Vanyan, L.L., 1989. Source field problems in northern parts of the Baltic Shield, *Phys. Earth planet. Inter.,* **53,** 337–342.

Padilha, A.L., Vitorello, I. & Rijo, L., 1997. Effects of the equatorial electrojet on magnetotelluric surveys: field results from Northwest Brazil, *Geophys. Res. Lett.,* **24,** 89–92.

Pirjola, R., 1992. On magnetotelluric source effects caused by an auroral electrojet system, *Radio Sci.,* **27,** 463–468.

Pirjola, R. & Vilhanen, A., 1998. Complex image method for calculating electric and magnetic fields produced by an auroral electrojet of a finite length, *Ann. Geophys.,* **16,** 1434–1444.

Quon, C., Vozoff, K., Hoversten, M., Morrison, H.F. & Lee, K.-H., 1979. Localized source effects on magnetotelluric apparent resistivities, *J. Geophys.,* **46,** 291–299.

Schultz, A. & Larsen, J.C., 1987. On the electrical conductivity of the Earth's interior I: mid-mantle response function computation, *Geophys. J. R. astr. Soc.,* **88,** 763–781.

Smith, J.T. & Booker, J.R., 1991. Rapid inversion of two and three-dimensional magnetotelluric data, *J. geophys. Res.,* **96,** 3905–3922.

Srivrastava, S.P., 1965. Methods of interpretation of magnetotelluric data when source field is considered, *J. geophys. Res.,* **70,** 945–954.

Tikhonov, A.N., 1950. On determining electrical characteristics of the deep layers of the Earth's crust, *Doklady,* **73,** 295–297.

Vilhanen, A., 1996. Source effect on geomagnetic induction vectors in the Fennoscadian Auroral Region, *J. Geomag. Geoelectr.,* **48,** 1001–1009.

Vilhanen, A., Pirjola, R. & Häkkinen, L., 1993. An attempt to reduce induction source effects at high latitudes, *J. Geomag. Geoelectr.,* **45,** 817–831.

Vilhanen, A., Pirjola, R. & Amm, O., 1999. Magnetotelluric source effect due to 3D ionospheric current systems using the complex image method for 1D conductivity structures, *Earth Planets Space,* **51,** 933–945.

Wait, J.R. & Spies, K.P., 1969. On the representation of the quasi-static fields of a line current source above the ground, *Can. J. Phys.,* **27,** 2731–2733.

Wannamaker, P.E., Hohmann, G.W. & San Filipo, W.A., 1984. Electromagnetic modeling of 3D bodies in layered earths using integral equations, *Geophysics,* **49,** 60–74.

Wannamaker, P., Stodt, J. & Rijo, L., 1987. A stable finite element solution for two-dimensional magnetotelluric modeling, *Geophys. J. R. astr. Soc.,* **88,** 277–296.

Weaver, J.T., 1994. *Mathematical Methods for Geo-electromagnetic Induction,* p. 316, Wiley, Taunton.